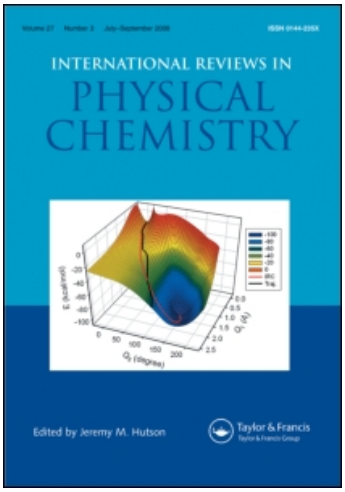


**International Reviews in Physical Chemistry**
Publication details, including instructions for authors and subscription information:
http://www.informaworld.com/smpp/title~content=t713724383

# Charge transfer in metal-atom-containing molecules in the gas phase

Niloufar Shafizadeh[a]; Benoit Soep[b]; Jean Michel Mestdagh[b]; W. H. Breckenridge[c]
[a] Laboratoire de Photophysique Moléculaire Bâtiment 210, Université de Paris-Sud, 91405 Orsay, Cedex, France [b] Laboratoire Francis Perrin (CNRS-URA-2453), DSM/IRAMIS/Service des Photons, Atomes et Molécules, France [c] Department of Chemistry, University of Utah, Salt Lake City, UT 84112-0850, USA

**To cite this Article** Shafizadeh, Niloufar , Soep, Benoit , Mestdagh, Jean Michel and Breckenridge, W. H.(2009) 'Charge transfer in metal-atom-containing molecules in the gas phase', International Reviews in Physical Chemistry, 28: 3, 359 — 406
**To link to this Article: DOI:** 10.1080/01442350903052663
**URL:** http://dx.doi.org/10.1080/01442350903052663

*International Reviews in Physical Chemistry*
Vol. 28, No. 3, July–September 2009, 359–406

Taylor & Francis
Taylor & Francis Group

# Charge transfer in metal-atom-containing molecules in the gas phase

Niloufar Shafizadeh[a], Benoit Soep[b]*, Jean Michel Mestdagh[b] and W. H. Breckenridge[c]

[a]*Laboratoire de Photophysique Moléculaire Bâtiment 210, Université de Paris-Sud, 91405 Orsay, Cedex, France;* [b]*Laboratoire Francis Perrin (CNRS-URA-2453), DSM/IRAMIS/ Service des Photons, Atomes et Molécules, C.E.A. Saclay, Bât 522, F-91191 Gif-sur-Yvette cedex, France;* [c]*Department of Chemistry, University of Utah, 315 S. 1400 East Room 2020, Salt Lake City, UT 84112-0850, USA*

(*Received 23 February 2009; final version received 14 May 2009*)

The presence of charge transfer (CT) is ubiquitous in metal-atom-containing molecules in the gas phase. The states of interest range from ground states to the lower excited states, given the generally low ionisation potentials of metal atoms. This review is written from an experimentalist's perspective, to describe the specifics of CT states in stable molecules containing a metal atom or of transient CT states in dynamical processes. The large body of experimental evidence allows the description of such states in an empirical or semi-empirical manner, including partial point charges and polarised electron clouds on the ions. These simple models are compared with more quantitative models, allowing the development of sophisticated descriptions. The simple perspective deriving from experimental evidence is justified, when it is possible via accurate quantum calculations and allows building a rather complete framework for the ionic bond or CT-induced dynamics.

**Keywords:** charge transfer; ionic bonds; harpoon mechanism; stereochemistry; quantum chemistry; calculations of charge transfer



## Contents

PAGE

**1. Introduction** 360

**2. Theoretical and experimental characterisation of CT in the gas phase** 362
2.1. A simple theoretical picture of the ionic bond 362
2.2. Experimental characterisation 367
2.2.1. Permanent CT states 367
2.2.1.1. Spectroscopic measurements 367
2.2.1.2. Deflection measurements 367
2.2.1.3. Indirect methods 368
2.2.2. Transient CT states 369
2.2.3. Tracking CT in excited states 369
2.2.4. Tracking CT States by photoionisation 371

*Corresponding author. Email: benoit.soep@cea.fr

ISSN 0144–235X print/ISSN 1366–591X online

DOI: 10.1080/01442350903052663
http://www.informaworld.com

2.2.4.1. Core electron ionisation 371
2.2.4.2. Direct ion-pair detection 372
2.2.4.3. Transient photoelectron spectroscopy 373

**3. Static interaction of metal atoms with electron acceptors (atoms and radicals)** 373
3.1. Acceptors with large positive EAs 373
3.1.1. Overview 373
3.1.2. Alkali mono-halides 375
3.1.3. Alkaline-earth monohalides 376
3.1.4. Summary for alkali monohalides and alkaline-earth monohalides 377
3.1.5. The concept of 'effective' polarisabilities 377
3.1.6. 'Pseudo-halides': hydroxides and methoxides 379
3.1.7. Low-lying excited states of alkaline-earth halides, hydroxides and $CaOCH_3$: quadrupole moment interactions 380
3.2. Acceptors with small positive electronic affinities: metal monohydrides and pseudo-hydrides 381
3.3. Transition metal monofluorides, monochlorides and monohydrides 382
3.4. Metal oxides: stabilisation of the $O^{-2}$ ion by metal ions 383
3.4.1. MO molecules 383
3.4.2. $M_2O$ molecules 386
3.4.2.1. Ground-state $Li_2O$ 386
3.4.2.2. The first electronically excited state ($\tilde{A}^1B_1$) of LiOLi 387
3.5. $M^+M^-$ excited electronic states 387

**4. Extension of the harpoon model: reaction dynamics of excited metal atoms and angle-dependent reactions** 388
4.1. The case of M*+HX(X = halogen) reactions 388
4.2. The angle-dependent harpoon model 392

**5. Dynamics of excited metal atom/molecule systems where the molecule has a negative EA** 394
5.1. Relaxation dynamics of excited metal atoms 394
5.2. Extension of the harpoon from a one-dimensional to a multidimensional model 395

**6. CT in excited states of large molecules containing metal atoms** 398

**7. Conclusions** 401

**Acknowledgements** 402

**References** 402

## 1. Introduction

A very important concept in the interaction of metal atoms with other atoms, small molecules or even large biological molecules in the gas phase is that of 'charge

transfer (CT)'. To what extent does a neutral metal atom transfer some of its electron density to the 'ligand' to which it binds, and how does this transfer depend specifically on the properties of the metal atom and the ligand?

The ionic character of a bond is central in the condensed phase, since ion chemistry drives many industrial processes and CT metal/molecule systems are at the heart of the cell's mechanism or atmospheric photochemistry. In the gas phase, the ionic character of a bond is directly observable for many experimental techniques but ionic bonds, in the absence of the stabilisation by a solvent, are less readily formed than in solution. Nevertheless, even in the gas phase, the electronic structure of bonds involving metals and the reaction dynamics of metal atoms include unavoidably some CT phenomena. For example, in many cases, metal–molecule reactions lead to ionic products from neutral reagents, thus a covalent-to-ionic crossing must occur, most likely at the transition state (TS) level. In the same way, most stable ionic metal salts do not correlate adiabatically to an ion pair system but correlates to neutral dissociation limits of lower energy via an ionic-neutral potential crossing. In this respect, static bond properties and reaction dynamics are intimately connected questions, which will be discussed here.

The idea of CT for metal/oxidant reactions was theorised very early in a simple model named the harpoon model that allows an oxidant to hook a metal via Coulombic interaction [1,2]. It has been extremely successful and served as a foundation for reaction dynamics since it allows a simple description of the forces ruling the dynamics at the TS level [3]. On the other hand, the partial ionic character of a chemical bond has been explored before [4] and the general structure of bonds with metals is of this nature. However, the quantitative theoretical description by quantum chemistry is extremely difficult to implement owing to the diffuse orbitals involved in the case of CT systems, even with the capabilities of present computers [5]. This leaves room for empirical and semi-empirical methods to pave the way for a more accurate description of the bonds in the ground and excited states of these molecules. A complete set of descriptions range between point charges and diffuse orbitals. In the same way, the dynamics of the CT in harpoon-type reactions is far more complex than the one-electron/one-dimensional approach between the reactants. This model along with experimental evidences, can involve several correlated electrons (excited state harpooning), several coordinates acting concertedly and reacting molecules with little electron affinity (EA). This has led to a more formal refinement of the simple model that is substantiated by the most recent calculations.

The present review is restricted to these aspects for metal–neutral molecule systems only for the sake of simplicity, since ion molecule systems have been extensively considered [6–8]. In addition, we shall not review here the dynamical aspects related to the ionic character which have been treated in many other instances [9,10]. From this perspective, this review is organised into two related parts: the static properties of ionic bonds involving metals and electron acceptors, and the transient CT states involved in metal–molecule reactions and in the collisional relaxation of excited metal atoms, or in metal-containing molecules. In the latter case of electronic excited metalloporphyrins (MP), the electron transfer from the porphyrin is the initial key mechanism, in the same way as the initial photo-induced electron transfer from chlorophyll drives the evolution in the photosynthetic reaction centre P680 [11].

## 2. Theoretical and experimental characterisation of CT in the gas phase

### 2.1. *A simple theoretical picture of the ionic bond*

The central focus of reaction dynamics is to uncover the motions of the constituent atoms in reacting systems. The theoretical approaches in this field always invoke the Born Oppenheimer approximation, which allows the separation between the electronic and nuclear motions. Accordingly, potential energy surfaces (PES) are obtained first by solving the electronic Schrödinger equation with fixed positions of the nuclei. Then, a treatment of the nuclear dynamics is performed, for example, by propagating wavepackets or by running trajectories on one or several PES's when the latter are coupled. Whatever is the intrinsic quality of the dynamical treatment, reliable results can be obtained only if the relevant PES's and couplings are described with enough accuracy on a wide range of geometrical arrangements, from the reactant valley to the product valleys through TS regions. Of course, the determination of the PES's does not need to be of the same quality over all the surface. Only the dynamically important regions need to be known very accurately. A 2008 state-of-the-art perspective on reaction dynamics can be found in the *Chemical Dynamics Special Feature* of the Proceedings of the National Academy of Sciences [12,13].

The task mentioned above is especially difficult with CT reactions, which is the focus of the present review. From reactants to products, the system experiences regions where the electronic configuration changes enormously. Technically, this implies that large configuration interaction treatments must be used to calculate the PES's. A recent review by G.-H. Jeung makes clear that having such information is often beyond the possibility of the current *ab initio* methods [5]. Attempts to perform such treatments are reported in Section 4 of the present review.

The present section examines a simpler, although challenging, situation: the building of an ionic bond between a metal–atom, which acts as the electron donor and an electron acceptor. Both ground and electronically excited states are considered.

Let us first consider the ground state MgH molecule. The ionisation energy (IE) of Mg is 737.8 kJ/mol [14] (The conversion of kilojoules per mole to the energy unit in electron volt is 0.01036410, thus the reader can apply a 1/100 factor if needed.). The EA of the H atom is about ten times smaller, 72.8 kJ/mol [15]. At infinite separation between Mg and H, the energy of the ion pair $Mg^+ + H^-$, is thus 665 kJ/mol above that of the Mg + H pair. As the Mg–H interatomic distance decreases, the Mg + H interaction energy decreases only slightly due to the van der Waals (and weak chemical) attraction of Mg and H. In contrast, the $Mg^+ + H^-$ potential energy drops substantially because of the strong Coulomb attraction between the positive and negative charges. Assuming a $1/R$ dependence of the $Mg^+H^-$ potential energy ($R$ is the Mg–H distance) and a flat MgH potential energy, the two potential curves that describe $Mg^+H^-$ and MgH cross each other at $R_{cross} = 0.209$ nm ($R_{cross} = 139/(IE - EA)$), where the IE and the EA are given in kilojoules per mole and $R_{cross}$ in nanometre), a distance larger than the equilibrium distance in MgH, 0.173 nm [16]. Both $Mg^+H^-$ and MgH have $^2\Sigma^+$ symmetry. In an adiabatic picture, their potential curves should not cross as $R$ is varied. Actually, the crossing discussed above is between two diabatic curves, which represent two different electron configurations of the system, namely $3s^2_{Mg}\ 1s_H$ for MgH and $3s_{Mg}\ 1s^2_H$ for $Mg^+H^-$. When adiabatic curves are considered, a mixing is assumed between these two configurations, resulting into an 'avoided' crossing at $R_{cross} = 0.209$ nm. The adiabatic

curves do not cross. The lower one describes the ground-state Mg–H interaction, whereas the other curve corresponds to an electronically excited state. Considering the ground state as Mg and H approach each other, the dominant electronic configuration is $3s^2_{Mg}\ 1s_H$ at large separation. On closer approach, there is a transfer of a valence electron from Mg to H at $R_{cross}$. Hence, at smaller R, the $3s_{Mg}\ 1s^2_H$ configuration becomes dominant, and the molecule gains the $Mg^+H^-$ character, essentially. The potential minimum will occur at a smaller distance $R_e$ where the repulsion between the electrons of $Mg^+$ and those of $H^-$ begins to increase faster than the Coulomb attraction between $Mg^+$ and $H^-$.

This qualitative picture shows that even the ground state of a very simple molecule like MgH needs a multi-configuration approach to be described over a wide range of distances. Only two configurations are considered in the simple discussion above, $3s^2_{Mg}\ 1s_H$ for MgH and $3s_{Mg}\ 1s^2_H$ for $Mg^+H^-$. Actually, a reliable description of the MgH system must take into account that Mg, H, $Mg^+$ and $H^-$ are polarisable centres. As a result, *ab initio* investigations of these molecules require extensive configuration–interaction calculations, often at the limit of the current computational capabilities [5].

An elegant way to investigate the electronic structure of molecules like MgH is to perform an *ab initio* calculation using the formalism of Durand and Barthelat [17], which describes core electrons by a pseudopotential, complemented by a core polarisation operator, hence reducing the electronic problem to calculations on the valence electrons. In the present case, the core is formed by the $Mg^{2+}$ electrons, hence reducing MgH to the three valence electrons. This allows for extensive configuration–interaction calculations such as those performed in [18] using the internally contracted multi-reference configuration interaction (IC-MRCI) method. The top panel in Figure 1 shows the first three $^2\Sigma^+$ potential energy curves of the MgH calculated in [18].



These three curves are essentially flat at long distance. At closer Mg–H distances, they exhibit strong avoided crossings, which follow the ion-pair curve describing the Coulomb attraction between 'unpolarisable' $Mg^+(3s\ ^2S)$ and $H^-$ ions. The bottom panel of Figure 1 shows the permanent dipole moment associated with these three states. As expected, their value is zero at large distance where the Mg and H interact only weakly. They show a negative value corresponding to the $Mg^{+\delta}H^{-\delta}$ dipole in the region of the avoided crossing mentioned above. The reason is found in the qualitative picture of the ionic bond described above. The strongly attractive configuration $3s_{Mg}\ 1s^2_H$ pushes down all the $^2\Sigma^+$ potential energy curves. This creates the well of the $1^2\Sigma^+$ curve at 3.25 $a_0$ and the series of avoided crossings. As can be seen when observing the variation of the dipole moments in the bottom panel of Figure 1, the regions of avoided crossing correspond to an exchange of the $Mg^+H^-$ between the two states that interact: the dipole along one curve decreases whereas the other one increases. The avoided crossing between the $1^2\Sigma^+$ and $2^2\Sigma^+$ states is directly responsible for the well at large distance in the $2^2\Sigma^+$ curve, at 4.90 $a_0$. The outer well in the $3^2\Sigma^+$ curve at 7.66 $a_0$ has similar origin, the avoided crossing between the $3^2\Sigma^+$ and $2^2\Sigma^+$ states. Let us follow the $3^2\Sigma^+$ state for decreasing Mg–H distances, starting at 15 $a_0$. Between 15 and 10 $a_0$ it receives a strong $Mg^{+\delta}H^{-\delta}$ character from the $4^2\Sigma^+$ state, which is not shown in the figure. Below 10 $a_0$, the $3^2\Sigma^+$ loses the $Mg^{+\delta}H^{-\delta}$ character to the benefit of $2^2\Sigma^+$, the dipole of which is decreasing. At the same time, the dipole associated with the $3^2\Sigma^+$ state increases and even becomes positive. However, at 4 $a_0$ the potential energy of the system is close to that of the excited $3p_{Mg}\ 1s^2_H$ configuration, which is strongly attractive since it is dominant in the $Mg^+(3p\ ^2S)$–$H^-$ ion pair. This is the origin

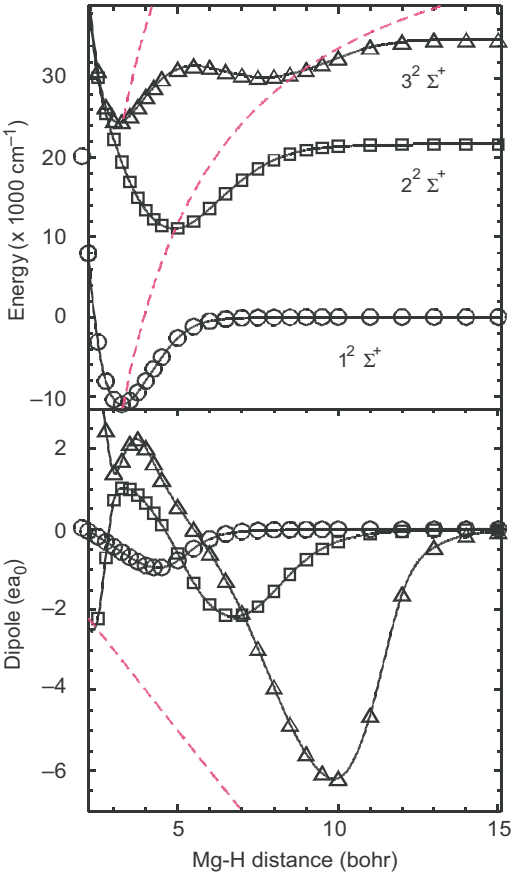


Figure 1. *Top panel*: 1, 2 and $3^2\Sigma^+$ potential energy curves of the MgH molecule as a function of the Mg–H distance, *R* (adapted from [18]). The solid lines passing through the calculated points are spline fits. The two dashed curves show the 1/R Coulomb potential energy associated with the $Mg^+(3s\ ^2S)$–$H^-$and $Mg^+(3p\ ^2P)$–$H^-$ ion pairs. *Bottom panel*: Permanent dipole moment of the same states. The dashed line shows the expected $Mg^+H^-$ dipole when a single electron is fully transferred from Mg to H.
*Note*: In both panels, the open circles, squares and triangles refer to the 1, 2 and $3^2\Sigma$ states, respectively.

of the inner well in the $3^2\Sigma^+$ curve, at 3.16 $a_0$. Interestingly, this well is almost a vertical translation of the ground state well in the $1^2\Sigma^+$ curve. This always happens in systems bonded by an ionic bond when the electronic excitation simply corresponds to the excitation of the positive moiety and not to a CT from the negative to the positive moiety.

A final remark must be made concerning the bottom panel in Figure 1: the calculated dipole moments are significantly smaller than expected in a crude picture where an electron is fully transferred from Mg to H. This has of course a simple physical origin: the electron cloud on one centre is polarised by the charge on the other centre. Hence, whatever the interatomic distance, the actual MgH system can never be described by the

interaction between +e and −e point charges separated by the Mg–H distance. This will be extensively discussed in Section 3.1. It is exemplified in the case of metal halides some of which are 100% ionic but, owing to charge distribution, do not have anything close to a point charge dipole. This point is important because it has been the focus of many discussions, whether retrodonation was at work or simply charge reorganisation (polarisation) around the negative ion [19].

It is important to emphasise that the present analysis of the MgH molecule is not specific to this particular system. A similar series of energy states coupled together by avoided crossing in regions of CT has been encountered and discussed along the same lines in the other alkaline-earth monohydrides: BeH [20], CaH [21–23], SrH [24] and BaH [25]. A similar situation is encountered in the alkali hydrides. Their ground states are of ionic character and dissociate into neutral fragments. Again, CT avoided crossings occur between states of the same symmetry. The corresponding literature is enormous and only the most recent *ab initio* studies are cited here: LiH [5,26], NaH [27], KH [28,29], RbH [30] and CsH [31,32] molecules.

The MgH molecule and more generally mono-hydrides could be considered as a special case with regard to the ionic bond concept since the EA of the H atom is not very large, 72.8 kJ/mol [15], compared to that of the halogen atoms, which is about five times larger [33]. This affects essentially the location of the switching region from covalent to ion-pair configurations and not the overall shape of the energy curves, comparing for instance the present Figure 1 to the Figure 1 of [34]. The latter reports a very recent all-electron treatment of the ground and low-lying excited potential energy curves of BaI by the MRCI method. The discussion drawn above for the MgH potential curves can be transposed easily to describe the potential energy curves of the BaI molecule. As we shall see now, it is useful also to the discussion of polyatomic systems.



Figure 2 shows cuts through the ground state and low-lying excited energy surfaces of the MgOH molecule. The calculation follows the same lines as those reported above for MgH. The formalism of Durand and Barthelat [17] allows reducing the electronic problem to the treatment of the valence electrons, nine in the present case. Again, the calculations are performed using the IC-MRCI method. The results shown in Figure 2 are close to those reported in [35], where an all-electron multi-reference double excitation configuration interaction (MRD-CI) approach has been used. The ground-state MgOH molecule at the equilibrium position has essentially the $Mg^+OH^-$ configuration. In linear and bent geometries, this corresponds to $\Sigma^+$ and A′ symmetries, respectively. At large separation between Mg and OH, the ground-state configuration corresponds, of course, to the $Mg(3s^2) + OH(X^2\Pi)$ asymptote, hence leading at finite Mg–OH distances to a Π state in linear geometry and to a pair of A′ and A″ states in a bent geometry. When considering adiabatic correlations, it appears that stretching the Mg–OH bond from the equilibrium position correlates adiabatically to the excited state $Mg(3s3p\ ^3P) + OH(X^2\Pi)$ of the separated pair in linear geometry, whereas it correlates to the ground-state $Mg(3s^2) + OH(X^2\Pi)$ pair in bent geometries. This behaviour is explicit when comparing the two panels of Figure 2. That doubly degenerated $^2\Pi$ curve crosses the $^2\Sigma$ curve in the top panel whereas the A′ component that emerges from the $^2\Pi$ curve in the bent geometry produces a strong avoided crossing with the A′ curve that emerges from the $^2\Sigma$ curve (see the bottom panel of the figure). This illustrates the strong dependence of the CT process when potential curves of different symmetries are involved. Of course, the anticrossing

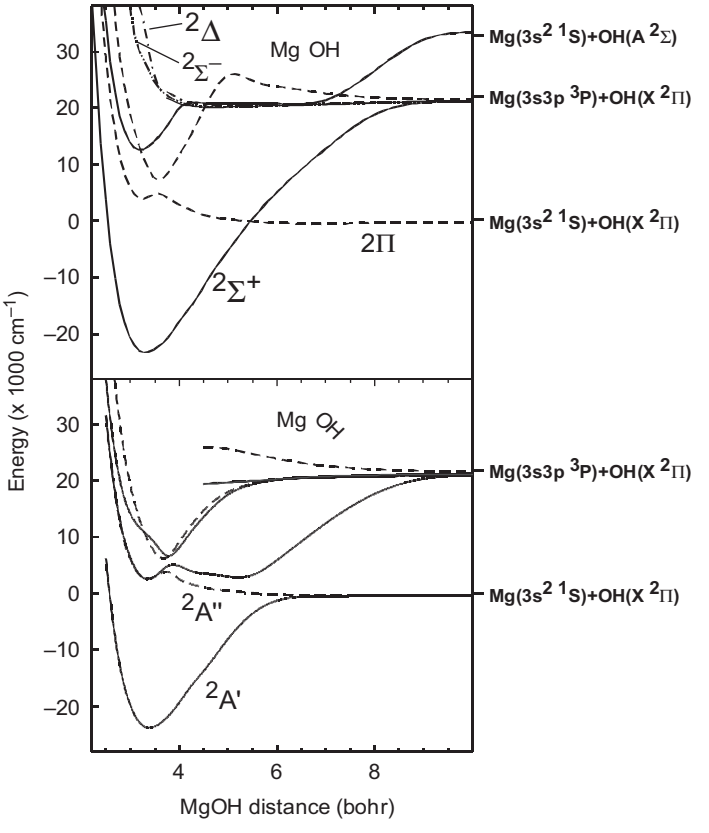


Figure 2. Cut through the potential energy surface of the MgOH molecule. The potential energy is plotted as a function of the Mg–O distance at a fixed O–H distance of 0.95 nm. The Mg–O–H bending angle is 180° and 135° in the top and bottom panels, respectively.

between the two $^2\Pi$ curve that appears in the linear geometry (top panel) is not affected significantly when the molecule is bent (bottom panel).

Let us consider for a while a dynamical problem where OH collides with Mg. If the Mg/OH system reaches the Mg–OH distance where the electron transfer is expected in a collinear geometry, the electron transfer will not occur for symmetry reasons and the collision will keep going on a covalent potential energy surface. In contrast, if the geometry is bent, the electron transfer can occur and the system is transferred to the ion-pair surface.

We conclude this section by observing that CT systems have a quite unique position in physical chemistry. We have seen already, and this review will illustrate this further below that a semi-quantitative description of the CT process is possible using very simple physico–chemical concepts based on electrostatics. This allows for a profound understanding of which important phenomena govern the experimental observation. This contrasts with the extreme difficulty of a quantitative description of these systems by *ab initio* methods, essentially because extensive configuration interaction is required, which often put the calculations at the limit of present computational capabilities.

### 2.2. *Experimental characterisation*

Charge transfer states are ubiquitous in living systems, stabilised by the solvent and mineral ions. They also exist in the gas phase, the central focus of the present review. There, they are difficult to characterise since these states sometimes correspond to excited states and are short or very short-lived. Let us thus divide their characterisation between permanent CT states (Section 2.2.1) and transient CT states (Section 2.2.2). Most of the methods rely directly or indirectly on the determination of the dipole moment, the quantum mechanical observable of the charge separation. CTs in electronically excited states are specifically examined in Section 2.2.3. Finally, detection methods probing the electron configuration directly, namely methods involving photoionisation and photoelectron spectroscopy, are presented as very promising tools for tracking CT states in Section 2.2.4.

#### 2.2.1. *Permanent CT states*

The most obvious method is to use the electrical properties of CT states: a large dipole moment resulting from the charge separation at large distances. The actual measured dipole moment results however, from different effects, the first one corresponding to the charge separation, the second to induction effects and the third to electron retrodonation as in Section 3.3 from a transition metal to a halide. Thus, the interpretation of the dipole moment is a difficult task that needs to be analysed theoretically. Besides, a molecule can exhibit charge separation and possess nonetheless a zero static dipole, such as linear molecules $B^-A^{++}B^-$ or $B^+A^- \ ^-B^+$.



2.2.1.1. *Spectroscopic measurements*. These measurements rely on the Stark effect, the splitting of rotational states into $2J+1$, $M_J$ states under the perturbation caused by the electric field: $H_{Stark} = -\mu E$. This splitting is different in different electronic states, hence spectroscopic measurements allow for the simultaneous determination of $\mu$ in both ground and excited states [36]. This method is extremely powerful and efficient in diatomic molecules and linear molecules but becomes difficult when the Stark splittings are small and the lines are ill-resolved. Hence, only pseudolinear molecules like $CaOCH_3$ have been investigated in this manner.

2.2.1.2. *Deflection measurements*. They rely on the Stark effect but only for the ground electronic state, where a rotational state $|J\,M_J\rangle$ of a dipolar molecule is selected. The molecule in this $|J\,M_J\rangle$ state is doubly deflected by an inhomogeneous electric field and hits a detector. In a Stark cell, intermediate in this device, the molecule is pumped from $M_J$ to $M'_J$ by a radio frequency source, in the presence of an electric field. The electric static field and the radio frequency field (RF) are set perpendicular to allow transitions with $\Delta J = 0$ and $\Delta M_J = \pm 1$. A specific $|J\,M_J\rangle$ state is focussed on the detector by a set of inhomogeneous fields. On resonance with the RF, the molecules in the $|J\,M_J\rangle$ state are defocussed on the detector causing a signal dip. By scanning the RF, one can derive the frequency $\Delta$ of the $JM_J \rightarrow JM'_J$ transitions. The calculation of transition frequency $\nu$ with a proper spin rotation Hamiltonian allows for the determination of the dipole moment in a similar way as in the preceding, for a molecule having electronic and nuclear

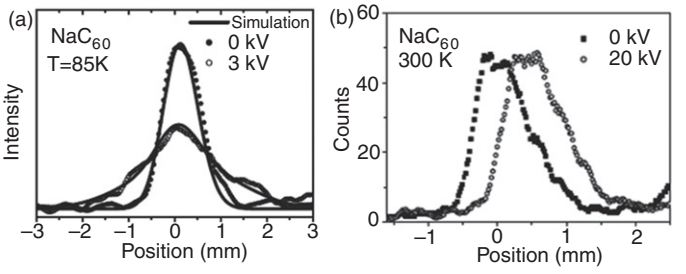


Figure 3. (a) Experimental beam profiles measured at 85 K for $NaC_{60}$ (symbols) and calculated profiles with $\mu = 14.8$ D (full line). (b) Experimental beam profiles measured at 300 K for $NaC_{60}$ [38].

spin moments. One obtains a transition frequency directly proportional to the square of the dipole moment of the molecule, $\nu \propto (\mu E)^2$, E being the Stark field. Thus, the dipole moment of caesium fluoride was measured as 7.3 D, indicating a strongly ionic bound molecule [37]. This method was used for a long time on salt molecules (metal ion halides) for which precise values of the dipole moment were determined. However, it is inapplicable to large molecules with dense rotational manifolds, where it is difficult to focus a single rotational level in this apparatus.

The original deflection method has been modified rather recently by using the deflection of dipolar molecules by a field gradient [38]. The force exerted on the molecule is $F = \mu\, \partial E/\partial x$ and recently developed systems provide very high-field gradients. However, this approach is not as simple as the preceding, since the dipole moments are randomly oriented and $\mu = \mu\langle\cos\theta\rangle$, thus the force averages over angles and applies to an ensemble of rotational levels. A classical simulation of the deflection of the molecule $NaC_{60}$ has been performed and is represented in Figure 3(a). It appears that the deviation is small but the broadening of the beam by the gradient is important.

For the example presented in Figure 3(a), the dipole moment is 14.8 D indicating a large electron transfer between sodium and fullerene [38]. Interestingly, the measurement was also performed at a different, higher temperature 300 K. A clear deflection then appears as shown in Figure 3(b). This is interpreted by the movement of the sodium atom on the surface of the fullerene owing to thermal energy and there exists in the presence of the electric field an apparently greater dipole moment [39]:

$$\mu = E\left[\frac{\langle\mu^2\rangle_T}{kT} + \alpha\right],$$

where $\alpha$ is the polarisability of fullerene (80 $\text{Å}^3$) and $\mu_T^2$ is close to the preceding value at 85 K.

2.2.1.3. *Indirect methods.* A systematic study of the CT properties in various complexes of electron donors with electron acceptors, has been performed by Legon [40] by rotational spectroscopy (pulsed Fourier transform, of the free-induction decay of the rotating molecule, thus transposing time oscillations of the electric field into frequency components). The electron transfer is monitored here via the hyperfine splitting observed in these spectra. In an atom, the nuclear quadrupole interacts with the field gradient of

Table 1. Quadrupole coupling constants of $^{35}Cl$.

| Molecule | Most important electronic structure | Quadrupole coupling constant $e \cdot q \quad Q$ in MHz |
|---|---|---|
| $Cl^{\bullet}$ | | −110.4 |
| ICl | I–Cl | −82.5 |
| ClCN | C≡N–Cl | −83.2 |
| $CH_3Cl$ | $H_3C$–Cl | −75.13 |
| NaCl | $Na^+Cl^-$ | <1 |

unpaired electrons in its vicinity, since paired electrons show an isotropic field. This thus provides an accurate measurement of the charge distribution around this atom. The hyperfine splitting, precisely measured with microwave accuracy, yields the hyperfine coupling constant $\chi = e \cdot q \cdot Q$ ($e$ is the proton charge, $Q$ is the nuclear quadrupole and $q$ is a quantity depending upon the charge distribution close to the nucleus). In this case, $q$ relates to the average field gradient $\langle \partial^2 V/\partial r^2 \rangle_{ave}$ about the atom.

In a method originally developed by Townes and Dailey [41], $q$ is then measured in molecules where the atom is bound within a chemical bond. However, on average, the unpaired electron remains about this atom and the wavefunction of the valence electron can be expanded as a linear combination of atomic orbitals. In the case of Cl, the atom that accepts a second charge as $Cl^-$, becomes spherically symmetric with $q = 0$. In an intermediate case where the molecule is partially ionic, the wavefunction is a superposition of neutral and ionic contributions with probabilities $1 - x$ and $x$, respectively. Hence, $q$ becomes a linear combination of the neutral and ionic contributions which can be disentangled. This has been successfully applied to radicals of increasing electronegativities [41] as show in Table 1. As expected, the $q$ value of $^{35}Cl$ in NaCl (i.e. $Na^+Cl^-$) is close to zero.



### 2.2.2. *Transient CT states*

Transient CT states show up when two species collide with each other. Many such situations are rationalised within the concept of the harpoon mechanism in which a metal atom + molecule reaction proceeds via the charge donation from the metal to the molecule. Thus, the TS is located in a potential energy region at the seam of the neutral reagents and in this CT curve. We shall discuss in Section 4 this mechanism which is based upon observations by Polanyi [1] and further substantiated by Maya [42] on the reactions of molecular bromine with alkali metals. The cross-sections are beyond 100 $Å^2$ corresponding to much larger distances between reagents than the normal onset of chemical forces. Also, the reaction cross-section increased for a series of reactions of $Br_2$ with the alkali metals correlatively with the decrease of the ionisation potential of the metal atom, from sodium through caesium. This is as expected if the cross-section of the reaction is determined by the electron capture distance by the halogen molecule from the alkali metal.

### 2.2.3. *Tracking CT in excited states*

In the case where the state of interest is no longer the ground state, it is necessary to employ different methods to characterise the CT. If one knows precisely the energy of the

CT state, a direct spectroscopic measurement would identify it readily. This is not generally the case except for X-ray absorption (or fluorescence or photoelectron spectroscopy). Most of the methods are indirect and employ spectroscopic tools that are sensitive to charge separation. Among the best studied systems are the molecules subject to intermolecular charge transfer (TICT) by twisting it along its axis and excited state proton transfer (ESPT) in clusters. In both cases, solvation by several molecules is necessary to accomplish the CT in the gas phase. One of the most common methods of investigation has been luminescence, following the example of Förster [43] who determined that naphtol was an excited state acid, that separated into $NaphtO^-$ and $H^+$, following the scheme described in Figure 4(a). Here by excitation of naphtol in solution, an excited naphtolate results in a stabilised form that fluoresces to a destabilised ground state. Thus, very important red shifts of the fluorescence were taken in this case as the characteristic of the formation of the ion pair.

Similar studies have been performed in gas phase clusters of 1-naphtol with ammonia by Leutwyler *et al*. [44]. It clearly appears that the fluorescence of small clusters (1 to 3–4 clustered ammonia molecules) the emission spectrum is characteristic of the resonant emission is typical of a van der Waals cluster, while beyond $n_{solvent} = 4$–5, the emission becomes strongly red shifted (by $9000\,cm^{-1}$) and diffuse. In the same way, absorption spectra, as taken by tuneable multiphoton absorption spectroscopy, reveal a completely diffuse spectrum for 1-naphtol-$(NH_3)_4$, in difference with the structured absorption of the smaller complexes. These systems are really the epitome of the observation of charged pairs in the gas phase. The latter spectroscopic method, invoking the great diffuseness of



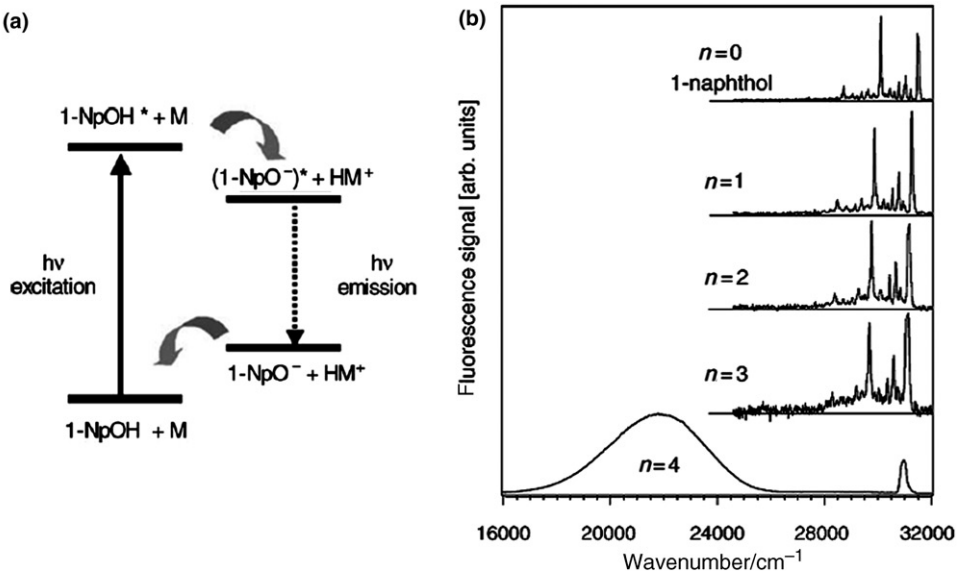


Figure 4. (a) Schematic energy diagram of the excitation mechanism and emission mechanism via the formation of a naphtolate $^-MH^+$(protonated solvent) ion pair. (b) Emission spectra of naphtol ammonia clusters labelled by the number of solvent ammonia molecules; the radical change in emission is seen at $n = 4$ [45].

spectra has to be complemented by systematic size or solvent comparisons, and of course calculations, since diffuseness in the spectra does not have CT as the only cause. The stabilisation observed in emission is simply much greater than that of an excimer.

### 2.2.4. *Tracking CT states by photoionisation*

2.2.4.1. *Core electron ionisation.* This method has yet only been used in solutions but can serve as an example. The basis of the measurements relies upon the change in the IE of a core electron 1s or 2s, 2p of a species (often a complex involving a transition metal atom) when its oxidation state is changed. In contrast to UV spectroscopy, X-ray absorption selects the properties of individual atoms. When metal complexes including surrounding ligands, such as bipyridil are investigated, it is possible to look at the specific properties of the metal atom. In these complexes, the change in oxidation state of the metal atom results from an electron transfer from the metal to surrounding ligands, for example, $Ru^{II}$ and $Ru^{III}$ complexes exhibit pronounced differences in their L-edge [46]. This is shown in Figure 5(a) and (b) for solution measurements of aqueous $Ru^{II}bipyridil_3^{2+}$: an absorption feature at 2841.0 eV (B), characterises the bivalent compounds due to the $2p_{3/2} \rightarrow 4d_{3/2}$ ($e_g$) transition next to the weaker $2p_{3/2} \rightarrow 5s_{1/2}$ transition around 2851 eV (C). The laser excitation removes the weakest bound electron from the fully occupied 4d ($t_{2g}$) level and generates a trivalent ruthenium compound, opening up an additional absorption due to



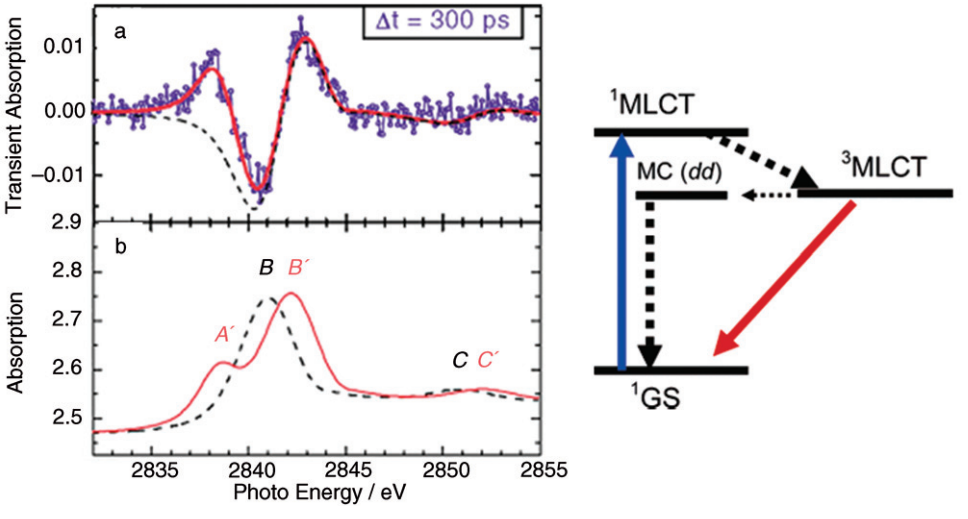


Figure 5. (a) Transient absorption spectrum of photoexcited aqueous $Ru^{II}bipyridil_3^{2+}$ (open circles) recorded 300 ps after the laser pump pulse. The dashed curve is a fit accounting for the blue shift of the static XAS due to the photo-induced increase of oxidation state, and the solid fit includes the appearance of feature A′ for the reaction intermediate. (b) Reactant $Ru^{II}$ state absorption spectrum (dashed) fitted from the experimental data, and the intermediate compound absorption spectrum (solid curve) constructed from the reactant state and the transient absorption fit, solid curve in (a), adapted from [46]. (c) The labelled features A′, B′, C′ and B, C denote the allowed transitions of $Ru^{III}$ and $Ru^{II}$, respectively. (d) Schematic photochemical cycle in $Ru^{II}bipyridil_3^{2+}$.

the allowed $2p_{3/2} \rightarrow 4d_{5/2}$ ($t_{2g}$) (A), in addition to the shift induced by the change in oxidation state.

In a pump probe experiment where the pump laser promotes a d electron to a CT state, a metal-to-ligand charge transfer (MLCT) occurs (Figure 5(c)), where the bipyridils share the charge, and the oxidation state of Ruthenium has changed to III. This transition at the blue edge of the visible spectrum is well-known and has been characterised for ruthenium asymmetric complexes by the Stark effect [47]. When this $^1$MLCT state is excited by a femtosecond laser and probed by X-ray pulses from a synchrotron source, after 100 fs the transient difference spectrum in Figure 5(a) corresponds to the decrease of feature B ($Ru^{II}$) and the appearance of the A′B′ doublet structure in the $Ru^{III}$ complex together with a ca. 1 eV shift in C′, resulting from the change of oxidation state of the ruthenium central atom in the formation of the CT state $^3$MLCT. Hence the transitions 'localised' on the metal help the direct characterisation of the electronic state of the metal and thus the change in charge distribution in the complex.

This method has been applied to solution systems and also to crystalline systems but by the use of photoelectron spectroscopy, it could easily apply to gas phase, more dilute samples of coordinated metals, provided they could be vaporised intact.



2.2.4.2. *Direct ion-pair detection*. If charges are separated in a state that correlates to $A^+ + B^-$, this state can be excited in such a manner that the energy is greater than its dissociation limit, and it is possible then to observe each of the separated ions $A^+ + B^-$, showing the true identity of this state. This dissociation limit lies above the ionisation limit of the AB molecule if the EA of B is lower than the $(A\text{-}B)^+$ bond energy. The observation of levels below the energy of the charge separated ions $A^+$ $B^-$ has been compared to the observation of Rydberg states with a heavy electron (the anion) [48]. An example is given here on a simple diatomic oxygen whose CT separation limit lies 1.45 eV below the dissociative ionisation limit, at 18.73 eV into $O^+(^4S) + O(^3P)$ [49]. In Figure 6, the separated ions are excited by three photons of a 205 nm femtosecond laser directly in the repulsive limb of the $O^+ + O^-$ potential, ~0.9 eV above the ion-pair asymptote (Figure 6(b)). The kinetic energy of the recoiling ion pair appears in the images in the

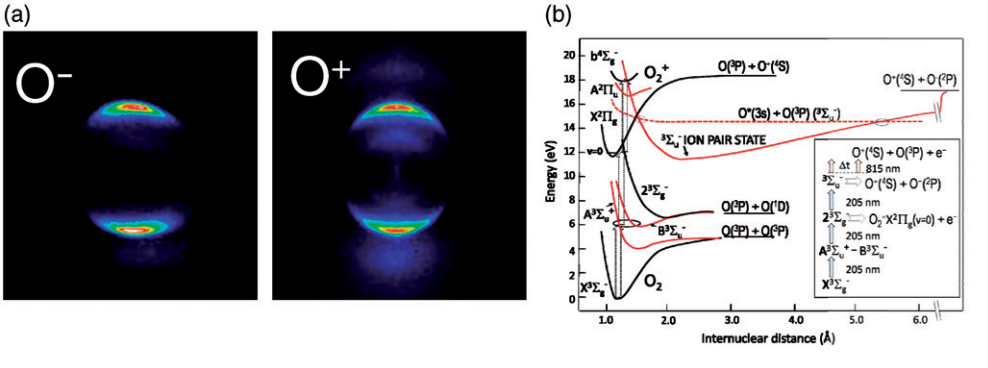


Figure 6. (a) Velocity map images of $O^+$ and $O^-$ ions arising from the photodissociation of $O_2$ pumped by femtosecond radiation at ~205 nm and three photons. (b) Relevant potential energy curves of the excited states of $O_2$ and $O_2^+$ in the energy region of interest [49].

size of the half circles in the images that are identical. The clouds of recoiling ions are oriented along the direction of the electric field of the laser.

This method, at this time has only been applied to simple molecules, although the observation of Coulomb explosion of 7-azaindole dimers to detect intermediate states is akin to it [50]. It could be applied to large polyatomic systems, the main difficulty being to achieve an absorption to the Franck–Condon disfavoured repulsive limb. Here for oxygen, this was done by exciting several steps including repulsive states of oxygen.

2.2.4.3. *Transient photoelectron spectroscopy*. In photoelectron spectroscopy of CT states in molecules, one cannot rely, as for the 'local X-ray ionisation' of a metal embedded in an organometallic complex, on the difference in the ionisation potential to discriminate this state from the others. However, molecules can exhibit several ionisation limits converging to ground or excited state ions. This follows Koopman's theorem describing the ionisation from the highest occupied molecular orbital in the system. In the pyrazine molecule, the excited states show two ionisation routes via the ejection of a $\pi^{-1}$ electron or $n^{-1}$ [51]. The different convergence limit can also be related to an excited ion if it differs in geometry from the neutral.

Charge transfer bears a resemblance to Rydberg states, via their Coulomb attraction potential, a resemblance already mentioned for ion-pair states and their dissociation. There the anion $B^-$ plays the role of a heavy electron [52,53]. Therefore, photoelectron spectra of these excited states, from the bound levels to the ionisation continuum of the neutral should resemble that of Rydberg states. In view of the preceding paragraph, the ionisation limit of the $A^+$–$B^-$ CT intermediate will relate to the ionisation limit of the $A^+$ moiety, or at least to the limit where the charge is borne by the A, $A^+$–B group [52,53]. A final word should be said about CT occurring between a Rydberg atom A and a molecule M. The higher ionisation potential of the molecule allows for the CT from the neutral Rydberg to the molecule forming after collision, a separated ion pair $A^+ + M^-$. Although this has not been applied to metal Rydberg states, it forms an interesting way to study electron transfer spectroscopy.

In conclusion, while most of these methods apply to bind CT states, the last one applies to recoiling charged separated fragments. Theory is of great help in all other cases despite the inherent difficulties to apply it to diffuse CT states.



## 3. Static interaction of metal atoms with electron acceptors (atoms and radicals)

### 3.1. *Acceptors with large positive EAs*

#### 3.1.1. *Overview*

Section 2.1 addresses the way an ionic bond is formed between a metal atom acting as an electron donor M and an electron acceptor X, leading to the dominant $M^+X^-$ configuration near the equilibrium geometry $R_e$ of the MX molecule. The same section also outlines, that simple arguments accounting for the electrostatic attraction between two point charges located at the atomic centres can be used to predict almost quantitatively the M–X distance $R_{cross}$ where the adiabatic potential energy curves describing the ground and low-lying excited states of the MX molecule show strong avoided crossings associated with the electron transfer from M to

X ($R_{cross}$(Å) = 1390/(IE(kJ/mol) − EA(kJ/mol)) = 14.4/(IE(eV) − EA(eV))), where IE and EA are the ionisation energy of M and the electron affinity of X, respectively). In contrast, the permanent electric dipole moment of the MX molecule at the equilibrium geometry is substantially smaller than expected from the simple point charge model.

The present section reviews experimental data on CT metal–ligand systems, dipole moments in particular, and discusses their values using more refined models, which account for the strong electrostatic effects that play a role near the equilibrium radius $R_e$ of strong MX ionic molecules. Dipole moments are indeed especially sensitive due to these effects, much more than the electron transfer radius $R_{cross}$. The charge on one ion induces a dipole moment on the other. This lowers the potential energy and contributes positively to the bond strength, but also tends to reduce the net dipole moment, since the two 'local' charge-induced dipoles on the $M^+$ and $X^-$ electron clouds will be opposite in sign to the main $M^+X^-$ 'point-charge' dipole. (A more 'chemical' explanation of this effect is that there is still some 'covalent' bonding in '$M^+X^-$'molecules (Table 2).)

So how much 'net' charge is really transferred in molecules like MX? One can get an experimental 'lower-limit' estimate for those MX molecules for which the dipole moments have been measured. According to [54],

$$\mu(\text{Debye}) = 4.80 \cdot R_e\,(\text{Å}) \cdot \delta \tag{1}$$

where $\delta$ is the net fraction of a unit charge transferred. Shown in Table 2 are some calculated values of $\delta$ for MX molecules, with some values of more covalent molecules included for comparison. It is obvious that the net CT in alkali halide diatomic molecules is substantial: greater than 0.7–0.9 units of CT, but the variations with M and X appear to be complicated, as expected, since they depend on the IE of M, the EA of X and the 'size' (affecting repulsion) and polarisability of both the $M^+$ and $X^-$ ions. Of course, it is also somewhat arbitrary as to how one assigns the 'net' charges on each ion, since there is obviously strong repulsive overlap of the electron clouds of the $M^+$ and the $X^-$ ions near



Table 2. Lower-limit fractional CT $\delta$ in diatomic molecules.

| Molecule | Average bond length (Å) | Dipole moment (D) | $\delta$ | Δ(EN) |
|---|---|---|---|---|
| NO | 1.154 | 0.16 | 0.03 | 0.40 |
| HI | 1.620 | 0.45 | 0.06 | 0.46 |
| CIF | 1.632 | 0.89 | 0.11 | 0.82 |
| HBr | 1.424 | 0.83 | 0.12 | 0.76 |
| HCl | 1.284 | 1.11 | 0.18 | 0.96 |
| HF | 0.926 | 1.83 | 0.41 | 1.78 |
| CsF | 2.347 | 7.85 | 0.70 | 3.19 |
| LiCl | 2.027 | 7.08 | 0.73 | 2.18 |
| KBr | 2.824 | 10.60 | 0.78 | 2.14 |
| NaCl | 2.365 | 8.97 | 0.79 | 2.23 |
| KCl | 2.671 | 10.23 | 0.82 | 2.34 |
| KF | 2.176 | 8.55 | 0.82 | 3.16 |
| LiF | 1.570 | 6.28 | 0.84 | 3.00 |
| NaF | 1.931 | 8.12 | 0.88 | 3.05 |

*Source*: [54].
Note: Δ(EN) is the difference in electronegativity of the two atoms.

the equilibrium bond distance of the $M^+X^-$ molecule – after all, that is what causes there to be a minimum in the potential curve!

### 3.1.2. *Alkali mono-halides*

The quantitative description of all the effects which contribute to the net dipole moments of alkali halide diatomic molecules is thus difficult, mostly due to the complexity of describing the electron-cloud 'overlap' of $M^+$ and $X^-$ ions at small $R$, but a lot of progress has been made in this area.

An early attempt to provide a semi-quantitative model for alkali–halide bonding, including the ion-induced-dipole polarisation effects, was that of Rittner in 1951 [55]. Using classical electrostatics, he derived equations for the induced ('back') dipole moments of the $M^+$ and $X^-$ ions in terms of a power series. Including only the first two terms of the power series, the net dipole moment of $M^+X^-$ molecules was predicted to be

$$\mu = eR - \left[\frac{R^4 e(\alpha_1 + \alpha_2) + 4\mathrm{Re}\alpha_1\alpha_2}{R^6 - 4\alpha_1\alpha_2}\right] \tag{2}$$

where $R$ is the distance between $M^+$ and $X^-$ nuclei, $\alpha_1$ and $\alpha_2$ are the effective polarisabilities of $M^+$ and $X^-$ at distance $R$, and $e$ is the unit charge. This early 'Rittner potential' model was qualitatively successful in predicting the decrease in dipole moments from those predicted by a complete $M^+X^-$ CT, but at the time there were only a few reliable experimental dipole moments available for alkali halide diatomic molecules in the gas phase to test the model comprehensively. Brumer and Karplus [56] later showed quantum mechanically that the true expression, at least at the reasonable limit of second-order perturbation theory, really equalled the first term in the power series, resulting in the simpler 'Truncated-Rittner' or T-Rittner equation for the overall dipole moment:

$$\mu = eR - \left[\frac{e(\alpha_1 + \alpha_2)}{R^2}\right] \tag{3}$$

As we shall see below, a second-order perturbation treatment, while apparently approximately valid for the alkali halides, where the polarisabilities of the alkali ions are quite small, is not an adequate approximation for metal halides where the polarisability of the metal ion is large (such as the alkaline-earth halides). Brumer and Karplus claimed that the T-Rittner model was superior to that of the Rittner model in many ways, but as Kumar and Shanker [57] later pointed out, they actually determined the 'effective' polarisabilities of $M^+$ and $X^-$ ions by fitting the experimental dipole moment values of several $M^+X^-$ molecules to Equation (3). Kumar and Shanker improved on this by calculating the 'effective' polarisabilities from the Pauling [4] free-ion polarisabilities in the Coulomb potential of the counter-ion at distance $R$, using the NR ion-dependent potential [57]. Using the Rittner model (Equation (2)) and the T-Rittner model (Equation (3)) and their calculated $\alpha_1$ and $\alpha_2$ values, they were able to fairly well reproduce $\mu$ values for 25 alkali halides [57]. Shown in Table 3 are the results. It appears difficult to tell whether the Rittner or the T-Rittner model is better, since both are quite satisfactory in predicting dipole moments at the bond distance $R_e$ for the alkali halide molecules.

Table 3. Values of calculated dipole moments $\mu$ in D [57].

| Molecule | Rittner model Equation (2) | T-Rittner model Equation (3) | Experimental |
|---|---|---|---|
| LiF | 6.15 | 6.20 | 6.28 |
| LiCl | 7.08 | 7.13 | 7.08 |
| LiBr | 7.12 | 7.17 | 7.22 |
| LiI | 7.32 | 7.38 | 7.42 |
| NaF | 7.95 | 8.06 | 8.12 |
| NaCl | 9.02 | 9.17 | 8.97 |
| NaBr | 9.14 | 9.31 | 9.09 |
| NaI | 9.40 | 9.57 | 9.21 |
| KF | 8.18 | 8.57 | 8.55 |
| KCl | 10.02 | 10.46 | 10.23 |
| KBr | 10.37 | 10.84 | 10.60 |
| KI | 10.91 | 11.40 | 11.05 |
| RbF | 8.00 | 8.53 | 8.51 |
| RbCl | 10.20 | 10.80 | 10.48 |
| CsF | 6.99 | 7.86 | 7.85 |
| CsCl | 9.95 | 10.84 | 10.36 |
| CsI | 11.33 | 12.30 | 12.10 |



### 3.1.3. *Alkaline-earth monohalides*

Just as for all the alkali halides, $R_{\text{cross}} \gg R_e$ for all the alkaline-earth halides (Mg to Ba). For the alkaline-earth monohalides, however, both the Rittner and the T-Rittner models fail dramatically in some cases. For example, the dipole moment of CaF has been measured [58] to be +3.07 D, but the T-Rittner and the Rittner models yield values of −0.32 D and −9.5 D, respectively [59]. This is because of the much larger polarisabilities of the alkaline-earth ions, which have single diffuse outer-shell ns electrons instead of the compact $(n-1)p^6$ filled-shells of the alkali ions. The necessary approximation $R^6 \gg 4\alpha_1\alpha_2$ (Equation (1)) is thus no longer valid.

Törring *et al.* [59,60] developed a simple model for the alkaline-earth halides, which allowed for the very large shift in electron density of the open-shell, polarisable $M^+(ns)$ outer electron away from the $X^-$ ion. The model is a modification of the Rittner model in which the $M^+$ ion is treated as an $M^{++}$ ion at a distance $R$ from the $X^-$ nucleus plus a negative charge shifted an amount $\Delta R$ away from the $M^{++}$ nucleus due to polarisation by the $X^-$ charge. The polarising field felt by the $X^-$ ion is thus a superposition of those due to the $M^{++}$ positive ion at $R$ and the $M^+$ negative electron at $R+\Delta R$. The field felt by the $M^+$ negative electron (simply assumed to be spherically symmetric about the point $\Delta R$ from the $M^{++}$ nucleus) is that due to the $X^-$ charge located at the $X^-$ nucleus ($\Delta R$ for the filled shell $X^-$ ion is thus assumed to be small compared to $R$, which is one of the Rittner approximations [55]. This was justified [59,60] by the fact that all six p-electrons contribute to the polarisability of the $X^-$ ion, so $\Delta R$ along the bond axis for the $X^-$ ion is much smaller). The resulting equations allow $\Delta R$ to be solved iteratively. (The 'effective' polarisabilities of the halide ions were those calculated by fitting the alkali halide dipole moment data to the Rittner equation [59,60].) The model was fairly successful in predicting the only dipole moments known at the time (experimental values in parentheses;

Debye): CaF: 3.34 (3.07); CaCl: 4.47 (4.27); CaBr: 4.80 (4.36). The experimental dipole moments are substantially less than predicted by complete $M^+X^-$ point-CT (~10–13 D), and these major effects are therefore very nicely rationalised by the large $\Delta R$ shift of charge on the polarisable alkaline-earth ions [59,60].

More sophisticated theoretical treatments of alkaline-earth halide diatomic interactions have been published: ligand-field treatments by Field *et al.* [61], and *ab initio* treatments by Yarkony *et al.* and others [62]. These treatments result essentially in the same qualitative conclusions about CT and polarisation of the $M^+$(ns) electron cloud as does the simpler Törring–Ernst model [59,60], but are much more difficult to implement, especially for the heavier $M^+$ and $X^-$ ions. The results in both of these treatments are discussed in terms of s, p, d mixing (hybridisation) in the $M^+$('ns') non-bonding molecular orbital in the field of the $X^-$ ion, resulting in severe distortion (polarisation) of the 'ns' electron away from the $X^-$ ion, substantially reducing the dipole moments. (However, in some cases, the calculated dipole moments are in worse agreement than the much simpler Törring–Ernst empirical model, although of course these models more accurately represent the 'shape' of the $M^+$ non-bonding electron cloud.) For example, the Yarkony [62] results for $CaCl(X^2\Sigma^+)$ yielded 71% 4s$\sigma$, 21% 4p$\sigma$ and 1% 3d$\sigma$ contributions to the $Ca^+$ non-bonding MO, essentially consistent with the experimental result of Bernath *et al.* [63] from magnetic hyperfine measurements of 75% 4s$\sigma$ and 25% 4p$\sigma$. The ligand-field approach [61] also yielded essentially consistent values of 79% 4s$\sigma$, 19% 4p$\sigma$ and 2% higher-lying $n\sigma$ Rydberg AOs.

It should also be noted that the experimental magnetic hyperfine measurements of all the CaX ground states [63] show definitely that the reduction of dipole moments from the $M^+/X^-$ 'point-charge' values is due to ion polarisations and not to ionic–covalent mixing of $M^+X^-$ and MX electronic configurations. We quote from [63]:

The halide nuclear spin acts as a probe of the size and shape of the unpaired spin-density present at the halide nucleus. The strongest indication that the CaX molecules are nearly perfectly $M^+X^-$ ionic is that the magnitudes of the magnetic hyperfine parameters ($b$'s) are less than 1% of the values calculated for neutral halogen atoms. This is consistent with almost complete localisation of the unpaired spin density on $Ca^+$.



### 3.1.4. *Summary for alkali monohalides and alkaline-earth monohalides*

The model calculations and the hyperfine experimental measurements indicate quite clearly that:

(1) Both the alkali halides and the alkaline-earth halides are diatomic molecules in which complete CT has occurred. They are essentially $M^+X^-$ molecules.
(2) The reduction of their dipole moments from that expected from 'point-charges' centred at the $M^+$ and $X^-$ nuclei at distance $R_e$ is due to ion-induced-dipole interactions, and not to 'partially covalent' character.

### 3.1.5. *The concept of 'effective' polarisabilities*

Perhaps the biggest problem in the Rittner model (and the modifications thereof) is that the polarisabilities of the $M^+$ and $X^-$ ions near $R_e$ of the $M^+X^-$ molecules must be substantially changed from the 'free-ion' $M^+$ and $X^-$ polarisabilities to get agreement with

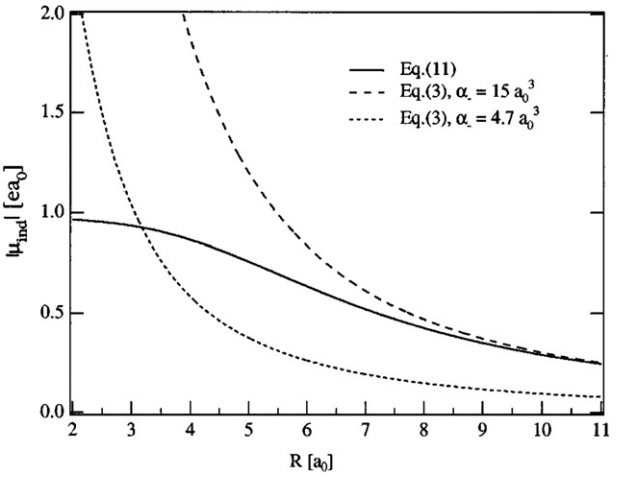


Figure 7. Calculated induced dipole on $F^-$ by a +2 point charge at a distance R. Dotted and dashed curves using constant polarisabilities in Equation (3), respectively $4.7a_0^0$ (the best-fit semi-empirical value used for $F^-$), and $15a_0^3$ (a typical *ab initio* value for $F^-$). The solid line is obtained using the method described in [65].



experimental dipole moment measurements. For example, for the alkali halides, where only the halide ions are very polarisable, the empirical 'best-fit' effective polarisability of $F^-$ is 0.70 Å [55,57] as compared to a good *ab initio* value of about 2.2 (Å$^3$) [64]. This 'best-fit' value is just what works best as a *single* value to rationalise the dipole moments of several alkali–ion $M^+X^-$ molecules with varying bond lengths $R_e$. The polarisabilities obviously vary with $R$, so this seems quite arbitrary and certainly could not be true at large $R$ (or small $R$).

The Kumar–Shankar treatment [57] was the first attempt to calculate $R$-dependent polarisabilities of the $X^-$ ions in the presence of $M^+$ ions. More recently, Field and Gittins [65] have presented a 'Hamiltonian' approach to calculating the effective polarisability of an $X^-$ ion in the presence of a $M^{+n}$ ion at a distance $R$. The authors estimated the effective polarisability of $X^-$ in the field of an $M^{++}$ ion by calculating the E-field-induced mixing of the $^1S$ and $^1P$ ground- and excited-state wavefunctions of the $X^-$ ions. This was done by constructing an effective $2 \times 2$ molecular Hamiltonian matrix which explicitly includes the $^1S$ and $^1P$ electronic states. The potential energy function for the $MX^+$ ion ground state is thus calculated as a function of $M^{++}/X^-$ distance $R$.

Shown in Figure 7 is the calculated [65] induced dipole on $F^-$ by a +2 point charge at distance $R$. Unlike the 'effective' polarisability model used by earlier workers, the calculated $\alpha$ of $F^-$ as a function of $R$ gives the correct 'long-range' dipole moment (using the 'free' ion polarisability of $F^-$) as well as the correct dipole moment near $R_e$ for $M^{++}/F^-$ ions. The induced $F^-$ dipole moment also 'saturates' correctly [65] at small $R$, rather than incorrectly approaching infinity.

Shown in Figure 8 is the potential curve for the $CaF^+$ molecule from the Hamiltonian treatment [65] versus a Morse curve constructed from the experimental spectroscopic values for $CaF^+$; the agreement is remarkably good near $R_e$ and $R < R_e$. (At $R > R_e$, of course, the curve incorrectly dissociates to $Ca^+ + F^-$, rather than Ca + F.) This method is

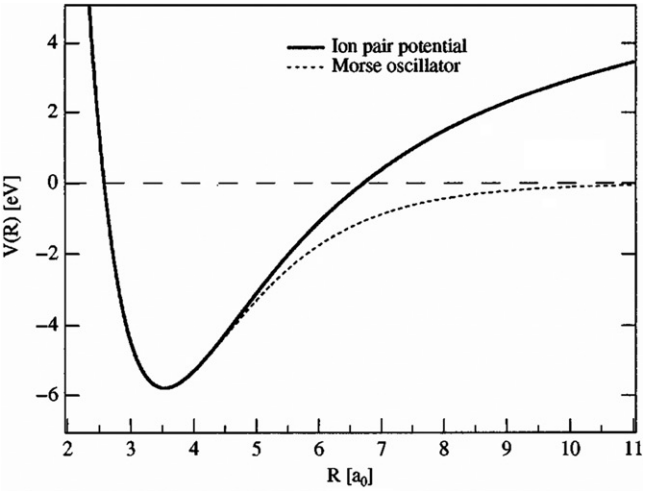


Figure 8. Potential energy curves for the ground state of $CaF^+$. The solid curve is the ion-pair potential and the dashed curve is a Morse potential resulting from the fit to the experimental data of [65].



thus highly promising, but as far as we have been able to determine, it has not yet been applied to any molecules other than the $CaF^+$ and $BaF^+$ ions in the original communication [65].

### 3.1.6. *'Pseudo-halides': hydroxides and methoxides*

Radicals like OH and $OCH_3$, also bond strongly and ionically with alkali and alkaline-earth atoms, since they have high EAs and are 'pseudo-halide' in electronic character. Mestdagh and Visticot [66] extended the Törring modification of the Rittner potential to alkali and alkaline-earth hydroxides. Firstly, they treated the $OH^-$ ion as an $(OH)^{+7}$ ion surrounded by eight polarisable electrons, similar to the Törring treatment of alkaline-earth ions as $M^{++}$ ions surrounded by a single polarisable electron. Secondly, they did not treat $(OH)^{+7}$ as a point charge, but as two point charges $O^{6+}$ and $H^+$, separated by the internuclear distance in the $OH^-$ ion. Thirdly, they assumed all the hydroxide molecules to be linear. Similar to the Törring model, then, when the $OH^-$ is polarised by the $M^+$ ion, the electronic charge on the $OH^-$ ion is shifted *towards* the $M^+$ ion by a distance $\Delta R^-$. (The treatment of the M+ ion was the same as the Törring model.)

Similar to the halide cases, the effective value of the polarisability used for $OH^-$ (1.2 Å$^3$) [55] had to be reduced significantly from the *ab initio* value for free $OH^-$ of 4.0 Å[55] in order to best fit all known or estimated dipole moments of the hydroxides known (*at the time*) [66].

Shown in Table 4 are the Mestdagh–Visticot 'predicted' semi-empirical [66] values of the dipole moments of the hydroxides compared to the currently accurately known experimental values [66]. The earlier predicted values are in reasonable agreement with, but somewhat lower than, the experimental values. The agreement can be greatly improved by slightly adjusting their earlier assumed value of 1.2 Å$^3$ for the effective value of the

Table 4. Values of dipole moments (D) 'predicted' by the Mestdagh–Visticot model.

| Molecule | Predicted values [66] | Experiment | New predictions |
|---|---|---|---|
| LiOH | 3.7 | 4.755 | 4.3 |
| NaOH | 6.4 | 6.832 | 6.7 |
| KOH | 7.2 | 7.415 | 7.5 |
| RbOH | 7.5 | | |
| CsOH | 7.4 | 7.1 (0.5) | 7.6 |
| MgOH | 1.2 | | |
| CaOH | 1.2 | 1.46 | 1.8 |
| SrOH | 1.8 | | |
| BaOH | 1.7 | | |

*Source*: [66].
Note: The new prediction column assumes an effective polarisability of $OH^-$ set at $1.0\,Å^3$ instead of $1.2\,Å^3$ in the original model.



polarisability of $OH^-$ to $1.0\,Å^3$ (Table 4). An *ab initio* calculated value [67] of the dipole moment of CaOH is only 0.98 D, substantially too low.

Steimle *et al*. [68] extended the Mestdagh–Visticot model to the pseudo-halide molecule $CaOCH_3$. (The $CH_3$ group was assumed to be a +1 point charge located at the C atom, which in fact may not be quite correct.) The model is less successful for $CaOCH_3$, predicting −0.1D versus the experimental value of $+1.58 \pm 0.08$D [68]. But the authors use a qualitative estimate of 3D for the effective dipole moment of the free $OCH_3^-$ ion which is based on an *ab initio* estimate of 2D for the $OCH_3$ radical [68]. If 2D were used instead of 3D, the predicted dipole moment for $CaOCH_3$ would essentially match the experimental value. Also, an assumed value of the effective polarisability of $OCH_3^-$ was partially based on the earlier assumed value of $1.2\,Å^3$ for $OH^-$ by Mestdagh and Visticot, so that using a new value of 1.0 Å [55] would presumably also increase the value of $\mu$ predicted for $CaOCH_3$ to a positive value more closely approaching 1.6D.

An attempt to predict the effective polarisabilities of pseudo-halides (as well as all the halides) as a function of $R$ in these ionic molecules, using perhaps something like the Field *et al*. [65] method would be a worthwhile endeavour, we believe.

Similar to the calcium halides, the magnetic hyperfine constants for the calcium pseudo-halides are all extremely small [68], further evidence that the unpaired electron lies completely on the $Ca^+$ ion (where $I = 0$).

### 3.1.7. *Low-lying excited states of alkaline-earth halides, hydroxides and $CaOCH_3$: quadrupole moment interactions*

The first excited states of alkaline-earth halides and pseudo-halides involve the interaction of excited $M^+((n-1)d)$ states instead of the $M^+(ns)$ ground states. These states have quadrupole moments, and the interactions of these quadrupole moments for $d\sigma$, $d\pi$, $d\delta$ alignments must be taken into account. Törring *et al*. [60] used a fitting procedure to obtain the effective $d\sigma$, $d\pi$, $d\delta$ polarisabilities and quadrupole moments which best reproduce all the known dipole moments and energies for the resulting $B\,^2\Sigma^+$, $A\,^2\Pi$ and $A'\,^2\Delta$ excited states of alkaline-earth halides. They utilised the well-known relations which

are derived from the angular parts of the free-ion d-orbital wavefunctions to reduce the number of free parameters to 2. Visticot and Mestdagh [66] extended this model to MOH molecules. Finally, Steimle [68] used the same procedure as Visticot and Mestdagh for the equivalent excited states of $CaOCH_3$. In general, the models were reasonably successful in reproducing the energies of these excited states as well as their dipole moments (when known).

### 3.2. *Acceptors with small positive electronic affinities: metal monohydrides and pseudo-hydrides*

The H-atom has an EA (+73 kJ/mol) [15] which is much less than the halogen atoms, but the monohydrides of alkali and alkaline-earth metal atoms still appear to be basically $M^+H^-$ in character. A calculation (Section 2.1) of the 'crossings', $R_{cross}$ of $M^+H^-$ ionic curves for all M = alkali and alkaline-earth metal atoms with the asymptotic energy M + H shows that $R_{cross}$ is always greater than the experimental $R_e$ for the neutral MH molecule.

However, because of the relatively high IE of the Mg atom, for MgH $R_{cross} = 2.09$ Å while $R_e = 1.73$ Å, so it is possible there is some mixed $MH/M^+H^-$ valence/ionic bonding character for MgH. This possibility is consistent with an *ab initio* analysis [69] of the charge densities of the second-row monohydrides, where NaH was clearly completely ionic, MgH and AlH were found to be 'transitional between the limiting classifications of ionic or covalent', and SiH, PH, SH and HCl were essentially covalent.

For the rest of the MH (M = alkali or alkaline earth) molecules, $R_{cross}$–$R_e$ varies from 0.85 Å to 2.10 Å, indicating these molecules are all essentially ionic.

Only for CaH has a dipole moment been characterised experimentally: $2.94 \pm 0.16$D [70]. Steimle *et al.* [70] showed that the Törring *et al.* [59] model can successfully reproduce this dipole moment if the effective polarisability of $H^-$ is reduced to 1.08 $Å^3$ versus an *ab initio* value of 1.69 $Å^3$ for the free $H^-$ ion [70]. (*Ab initio* calculated values of the dipole moment were somewhat low, ranging from about 2.3 to 2.7 D [70].) This allows predictions of dipole moments of other alkaline earth and alkali hydrides if experimental dipole moments are eventually measured. It is possible that even CaH has minor covalent character, however, since in contrast to CaX (X = halides), and CaOH, the magnetic hyperfine coupling constant for CaH is not extremely small [71], indicating that the unpaired electron spends a small part of its time on the H atom. High-level *ab initio* calculations indicate that the $CaH(X\,^2\Sigma^+)$ ground state is predominantly ionic, and that the low-lying excited states have unusual potential curves due to several ionic/covalent avoided crossings [72], similar to MgH (Section 2.1). There are other indications that the CaH ($X\,^2\Sigma^+$) ground state is greater than 90% $Ca^+H^-$ in character: an EPR study [73] of matrix-isolated CaH and an empirical deperturbation [74] of all the low-lying $^2\Sigma^+$ states of CaH.

Steimle [75] also measured the dipole moment of the $CaCH_3$ molecule, a 'pseudo-hydride', to be $2.62 \pm 0.03$D, a value similar to that of CaH. The model of Visticot and Mestdagh was applied to this molecule [75], by assuming that the valence electrons of the $CH_3^-$ ion were split into three equal point charges, each one positioned at a distance along the three C–H bonds. This distance was estimated by assuming each bond contributed equally to the $CH_3^-$ dipole moment, calculated to be 1.78 D. (This $CH_3^-$ dipole moment also contributes to the overall dipole moment of $Ca^+CH_3^-$, of course). The real unknown

was the effective polarisability of the $CH_3^-$ ion, for which even the 'free' value had not been calculated. Using 'free' values for isoelectronic $CH_4$ or $NH_3$ as approximations to the effective polarisability of $CH_3^-$ gave calculated values of 2.40 and 2.95 D, both in reasonable agreement with the experimental value of $2.62 \pm 0.03$ D. This may be by chance, since one would expect the polarisability of the negative $CH_3^-$ ion to be higher than that for $NH_3$ or $CH_4$, but the 'effective' polarisability for $CH_3^-$ in the $Ca^+CH_3^-$ ion should be slightly lower than that of the free $CH_3^-$ ion, thus the apparent agreement.

### 3.3. *Transition metal monofluorides, monochlorides and monohydrides*

Calculations comparing $R_{cross}$ ($M^+X^-/MX$) with $R_e$ are shown in Table 5 (as examples) for the second-row transition metal atoms, and X = F, Cl, H, where all $R_e$ values from Y to Pd have been calculated carefully and consistently via *ab initio* methods by Siegbahn [19].

Table 5. Calculations of $R_{cross}$ for transition metal MF, MCl and MH molecules.

| Species | $D_e$[a] (kJ/mol) | IP−EA (kJ/mol) | $R_{cross}$ (Å)[b] | $R_e$ (Å)[a] |
|---|---|---|---|---|
| YF | 661.8 | 288 | 4.83 | 2.00 |
| ZrF | 594.0 | 332 | 4.19 | 1.93 |
| NbF | 540.4 | 336 | 4.14 | 1.97 |
| MoF | 420.3 | 357 | 3.89 | 2.00 |
| TcF | 423.6 | 374 | 3.72 | 2.05 |
| RuF | 365.0 | 383 | 3.63 | 2.05 |
| RhF | 355.8 | 392 | 3.55 | 2.04 |
| PdF | 298.0 | 477 | 2.91 | 2.01 |
| AgF | 351.2 | 403 | 3.45 | 1.98 |
| CdF | 309.8 | 540 | 2.57 | – |
| YCl | 520.3 | 267 | 5.21 | 2.52 |
| ZrCl | 444.1 | 311 | 4.47 | 2.42 |
| NbCl | 422.8 | 315 | 4.41 | 2.46 |
| MoCl | 333.6 | 336 | 4.14 | 2.49 |
| TcCl | 346.6 | 353 | 3.94 | 2.54 |
| RuCl | 320.2 | 362 | 3.84 | 2.49 |
| RhCl | 325.7 | 371 | 3.75 | 2.46 |
| PdCl | 261.2 | 456 | 3.05 | 2.42 |
| AgCl | 310.6 | 381 | 3.65 | 2.28 |
| CdCl | 202.6 | 519 | 2.68 | – |
| YH | 284.6 | 543 | 2.56 | 1.96 |
| ZrH | 234.4 | 587 | 2.37 | 1.86 |
| NbH | 255.8 | 591 | 2.35 | 1.79 |
| MoH | 211.0 | 612 | 2.27 | 1.75 |
| TcH | 177.1 | 629 | 2.21 | 1.67 |
| RuH | 246.6 | 638 | 2.18 | 1.65 |
| RhH | 268.3 | 647 | 2.15 | 1.57 |
| PdH | 213.9 | 732 | 1.90 | 1.54 |
| AgH | 220.2 | 658 | 2.11 | 1.62 |
| CdH | 65.3 | 795 | 1.75 | 1.78 |

Notes: [a]From [19], except for AgX and CdX, which are from [76].
[b]$R_{cross}$ (Å) $= 1390 \cdot \left(\frac{1}{IP(M)-EA(X)}\right)$

Also shown in Table 5 are similar $R_{cross}$ calculations for the analogous AgX and CdX molecules, where experimental De values (where known) are taken from Huber and Herzberg's book [76]. It can readily be seen that for all the fluorides and chlorides $R_{cross} \gg R_e$, indicating that there is a substantial ionic component to transition metal monohalide bonding, as expected. The MH molecules also mostly have $R_{cross} > R_e$, but the $R_{cross}$–$R_e$ differences are much smaller, indicating that there may be 'mixed' ionic/covalent character in the ground-state wavefunctions, in agreement with Siegbahn's findings [19]. In fact, for CdH, $R_{cross}$ and $R_e$ are essentially identical, and the bond energy of CdH is quite small, indicating that the CdH molecule may be covalent in character, with the bonding only facilitated by unfavourable s-p$\sigma$ promotion on the Cd atom. This is likely to be true as well for the analogous ZnH and HgH molecules, which also have very weak bonds [76], and is consistent with conclusions from *ab initio* calculations [77–79]. Finally, the adiabatic ground-state potential curves of CdD and ZnD determined spectroscopically show unusually high anharmonicity [80], consistent with a strong avoided crossing between an attractive diabatic covalent state correlating with excited state M(ns np)+H, and a repulsive diabatic covalent state correlating with filled-shell ground-state M($ns^2$)+H.

Transition metal atoms form extremely strong bonds with halogen atoms, especially for those atoms to the left side of the nd rows. As an example, the bond energies of second-row MX molecules are displayed [19] in Table 5. Yttrium binds with fluorine by more than 660 kJ/mol. The binding of these systems, although very ionic, since their electronic states correlate with those of a $M^+$ ion (and the spin orbit coupling reflects that of the ion), cannot be entirely explained by a simple $M^+X^-$ interaction, however [19]. As an example, the binding energy difference between YH and YF is 377 kJ/mol (3.9 eV), while the EA difference between hydrogen and fluorine is $0.75 - 3.45 = 2.70$ eV. This bond energy difference, then, cannot be entirely accounted for by the greater EA of fluorine, given the identical bond lengths of both compounds. Besides, Mulliken electron densities, although inaccurate, indicate a fairly low charge on the metal for MX molecules [19].

It has been concluded [19] that lone pairs play an important role in the bonding: donation of halide ion lone pairs to empty d orbitals on the $M^+$ ions, such as in Yttrium, can lead to significant 'extra' bonding and partial neutralisation of the central metal ion. This aspect of metal monohalide bonding is unique to transition metal-type atoms [19]. Also, this kind of directional p$\sigma$/d$\sigma$ and p$\pi$/d$\pi$ 'back-donation' type of ligand bonding is not favourable for the diffuse, symmetric 1s orbital electron on $H^-$ ions, consistent with the lower bond strengths of MH molecules.

### 3.4. *Metal oxides: stabilisation of the $O^{-2}$ ion by metal ions*

#### 3.4.1. *MO molecules*

Considering that the O atom is the second most electronegative atom after the F atom [54], it is surprising that the EA of the O atom is so low, only 141 kJ/mol [54] compared to the halogen atom values of around 300 kJ/mol [54]. This is apparently due to the difficulty of simply adding another electron to the small O-atom-outer-shell, because of electron–electron repulsion (the larger S, Se, Te atoms in fact have greater EAs of around 190–200 kJ/mol [54]). For M atoms with relatively low first ionisation energies, MO molecules are essentially $M^+O^-$ in character, similar to the metal halides and the metal

Table 6. Calculated distances at which the $M^+O^-$ curves dip below the M + O asymptote, and distances at which the $M^+O^-$ and $M^{+2}O^{-2}$ curves cross, compared to the $R_e$ values (Å).

| Molecule | $R_e$ | $R_{cross}$ ($M^+O^-$/MO) | $R_{cross}$ ($M^+O^-/M^{+2}O^{-2}$) |
|---|---|---|---|
| LiO | 1.70 | 3.65 | 0.54 |
| NaO | 2.05 | 3.87 | 0.83 |
| KO | 2.22 | 4.98 | 1.18 |
| RbO | 2.28 | 5.31 | 1.34 |
| MgO | 1.75 | 2.32 | 2.16 |
| CaO | 1.82 | 3.10 | 2.57 |
| SrO | 1.92 | 3.40 | 2.70 |
| BaO | 1.94 | 3.84 | 2.89 |

hydrides discussed above. Due to the small size of the O-atom, the Re values of the diatomic metal oxides are relatively small, so the $R_{cross}$ values for the $M^+O^-$ curves are generally much greater than the $R_e$ values. In fact, the analogous $R_e$ values for MH and MF molecules for alkali metals are quite similar to those for the MO molecules.

The MO attractive potential energy (related to M + O) is:

$$E(M^+O^-) = \frac{-1390}{R} + IE(I) - EA(I), \tag{4}$$

where R(Å) is the M–O distance, IE (kJ/mol) is the first IE of M, and EA (kJ/mol) is the first EA of the O. Setting this equation equal to zero, one can calculate $R_{cross}$ ($M^+O^-$/MO), that is, where the $M^+O^-$ attractive curve dips below the M + O asymptotic energy. As can be seen in Table 6, for all the alkali and alkaline-earth monoxides, $R_{cross} \gg R_e$, indicating ionic bonding. So, there is little doubt that most such MO molecules have substantial ionic character, similar to the halides MX and most hydrides, MH, as discussed above.

But a more interesting possibility exists for some metal monoxides when the sum of the first and second ionisation energies of the metal atom is not too high: '$M^{+2}O^{-2}$' character at $R_e$. We do not examine this possibility for all metals, but focus here on the alkaline-earth metal atoms, which have a natural tendency towards a 'valence' of +2 because the second IE is relatively low for the outer $M^+$(ns) electrons [81]. At first glance, $O^{-2}$ character in such MO molecules might seem unlikely, since the EA of the $O^-$ ion is known to be substantially negative, around −5 eV (−482 kJ/mol) [82,83]. This means that the free $O^{-2}$ ion is not stable. However, as in the solid state, where many metal oxides appear to consist of $O^{-2}$ ions surrounded by a stoichiometric number of positive metal ions [84], the strong Coulombic attraction between +2 and −2 ions (four times as strong as that between +1 and −1 ions) can stabilise the $O^{-2}$ ion at small $R_e$ values. The $M^{+2}O^{-2}$ attractive potential relative to M + O is:

$$E(M^{+2}O^{-2}) = \frac{-(4)\cdot(1390)}{R} + IE(I) + IE(II) - EA(I) - EA(II), \tag{5}$$

where $R$(Å) is the MO distance, IEs are the first and second ionisation energies of M, and EAs are first and second EAs of O (in kJ/mol). Now, what matters in indicating $M^{+2}O^{-2}$

character for MO molecules near $R_e$ is whether the $M^+O^-$ or the $M^{+2}O^{-2}$ energy is the lowest at the $R_e$ of the MO molecule. Although the $M^{+2}O^{-2}$ potentials are four times more attractive due to the +2 charges, their asymptotes at larger $R$ are also much higher in energy, since the EA of $O^-$ is substantially negative, and the IE of $M^+$ has to be added in as well. But given the much stronger attraction, the $M^{+2}O^{-2}$ attractive curves will cross the respective $M^+O^-$ curves eventually at some $R$, even if it is at a quite unrealistically small value of $R$. However, if that crossing, $R_{cross}(M^{+2}O^{-2}/M^+O^-)$, occurs at a value much *greater* than the $R_e$ of the MO molecule, this will be a good (if qualitative) indicator that the MO molecule has substantial $M^{+2}O^{-2}$ character near $R_e$. By setting Equations (4) and (5) as equal, we can solve for $R_{cross}(M^{+2}O^{-2}/M^+O^-)$. Values thus calculated for the alkali and alkaline-earth monoxides are shown in Table 6. $R_{cross}(M^{+2}O^{-2}/M^+O^-)$ values for the alkali metals are very small, and much less than the $R_e$ values, as expected, since the IEs of the filled-shell $M^+$ ions are extremely high due to their 'inert-gas' electron configurations. In contrast, all of the $R_{cross}(M^{+2}O^{-2}/M^+O^-)$ values for the alkaline-earth MO molecules are substantially greater than the $R_e$ values, a very strong suggestion that $M^{+2}O^{-2}$ ionic character may dominate near $R_e$ for these molecules. Such $M^{+2}O^{-2}$ character may also be present in other MO molecules in which the sum of the first and second ionisation potentials of the M atom are not too high and the $R_e$ values for the MO molecules are fairly low, but for the sake of brevity, we do not extend the above analyses to other metal atoms.



A careful, high-level *ab initio* calculation [85], in which all the low-lying diabatic and adiabatic potential curves of MgO were included, from small to large $R$, shows that the ground-state MgO wavefunction is indeed dominated by the lowest-energy $6\sigma^2$ configuration at $R_e$, which is $Mg^{+2}O^{-2}$ in nature. However, there is also a strong mixing (−25%) of the $6\sigma7\sigma$ configuration [83], which is $Mg^+O^-$ in nature, indicating that the predicted CT to form $Mg^{+2}O^{-2}$ is not quite complete at $R_e$, and that MgO is somewhere between $Mg^{+2}O^{-2}$ and $Mg^+O^-$ in character at $R_e$.

The dipole moment of $MgO(X^1E^+)$ has been determined experimentally, by Stark spectroscopy, to be $6.2 \pm 0.6$D [86]. Theoretical *ab initio* calculations are consistent, with values of 5.7D [87] and 6.1 D [85]. These values are much, much smaller than expected, of course, for $Mg^{+2}O^{-2}$, due to induction of a large oppositely charged dipole on the very large, polarisable $O^{-2}$ ion by the $Mg^{+2}$ ion, as discussed above for metal halides, but the Törring–Ernst model [59,60] has apparently not been applied to this molecule. Given the calculated $R_{cross}$ ($Mg^+O^-/Mg^+2O^{-2}$) values for CaO, SrO and BaO, compared to the $R_e$ value (Table 6), the ground-state wavefunction of these molecules should be even more dominated by the $M^{+2}O^{-2}$ configuration. The dipole moments of those molecules are indeed higher than that of MgO, with values in the 8–9D range [86]. In fact, Field *et al*. [82] used a ligand-field, integer-charge ionic model to de-perturb the lowest $E^+$ states to their diabatic $Ca^{+2}O^{-2}$ and $Ca^+O^-$ potentials, and found that the de-perturbed $Ca^{+2}O^{-2}$ lowest state (using a Rittner model potential) is quite similar to the spectroscopically determined potential of the $CaO(X^1E^+)$ ground state.

On the other hand, recent high-level *ab initio* calculations by Harrison *et al*. [88] show that because the empty 3d orbital on the $Ca^+$ ion is so low-lying (to quote them: 'clearly, Ca is a transition element in waiting!'). There in fact appears to be considerable 'back-donation' of $O^{-2}$ electron density into the Ca(3d) empty orbitals. (This is somewhat similar, of course, to the cases of the early transition metal halides, as discussed in

Section 3.3.) The population analysis indicates a net $Ca^{+1.2}O^{-1.2}$ ionic character, with essentially all the extra electron density on the Ca atom (compared to $Ca^{+2}O^{-2}$) being in 3d orbitals, not the 4s orbital. Thus, the bonding can be viewed as $Ca^{+2}O^{-2}$, in nature, but with quite significant back-donation of $O^{-2}$ into the empty $Ca^{++}$(3d) orbitals. Similar effects would be expected for SrO and BaO but would not, of course, play any role for MgO bonding.

### 3.4.2. *$M_2O$ molecules*

3.4.2.1. *Ground-state $Li_2O$.* We discuss here only the $Li_2O$ molecule, which has now been studied thoroughly experimentally [89], with high-resolution spectroscopy, laser-induced fluorescence and stimulated emission pumping; and theoretically [90], with very accurate *ab initio* calculations. Interestingly, in both cases, it was the light-atom nature of this molecule which facilitated a successful characterisation: the light Li-atom allowed characterisation of experimental rotational-level spacings and the light $Li_2O$ atoms allowed the highest levels of theoretical calculations to be performed.

Theory [90] and experiment [89] are in quite remarkable agreement, and show that ground-state LiOLi is linear, with a very short Li–O bond distance of $R_0 = 1.611 \pm 0.003$ Å [89]. Thus 'lithiated water' differs dramatically from the strongly bent valence isoelectronic molecule HOH, and it appears that this is due to the completely ionic $Li^+O^{-2}Li^+$ nature of the ground state, so that the two $Li^+$ ions avoid each other as much as possible, with an 180° bond angle. This is consistent with the *ab initio* calculations [90], which yield an effective (natural orbital) charge on the Li atom of 0.93, thus indicating nearly complete $Li^+O^{-2}Li^+$ CT. It is also consistent with an early beam-deflection experiment [91], which indicated a dipole moment very near zero, and thus a Li–O–Li bond angle of 180°.

However, the bending vibrational mode of Li–O–Li also has a very low fundamental frequency of 112 $cm^{-1}$, indicating that the ground-state bending potential surface is quite flat near $R_e$ [89] and that the 180° bond angle is therefore not that strongly favoured. Breckenridge *et al.* [89] rationalised this in the following way: because the $Li^+$ ions are on opposite sides of the large, polarisable $O^{-2}$ ion, net $Li^+$-induced polarisation of $O^{-2}$ is zero, and cannot further lower the energy, as is the case for $M^{+2}O^{-2}$ ions. But if the molecule bends, then there is a competition between $Li^+/Li^+$ repulsion (raising the potential energy) and very large net $Li^+$-induced polarisation of $O^{-2}$ (lowering the potential energy). It appears, then, that the $Li^+/Li^+$ repulsion is dominant, but only barely! A simple +1/−2/+1 point-charge model calculation of LiOLi at $R_e$ showed that the bending frequency would be about 480 $cm^{-1}$, very much higher than that observed. A rough estimate [89] of the ion-induced dipole term at the classical $v'' = 0$ turning point of about 160° was consistent with a lowering of the potential energy of ~300–400 $cm^{-1}$ from the simple $Li^+O^{-2}Li^+$ point-charge model, as required.

The attractive potential curve of the $Li^+O^{-2}Li^+$ ionic state, dissociating symmetrically and linearly to $2Li^+ + O^{-2}$, referenced in energy to $2Li + O$, is:

$$E(R) = \frac{+1390}{2R} - \frac{(4)\cdot(1390)}{R} + 2(\mathrm{IE}) - \mathrm{EA(I)} - \mathrm{EA(II)}, \tag{6}$$

where $R$(Å) = Li–O distance (and this distance is half of the Li–Li distance), IE is the first IE of the Li atom, and the EA(I) and EA(II) are the first and second EAs of the O-atom

(kJ/mol). The first term is the $Li^+/Li^+$ repulsion, and the second term is the sum of the two $Li^+/O^{-2}$ attractions. Setting $E(R)$ to zero, one can solve for $R(\text{crossing}) = 3.42$ Å, which is very much larger than the Li–O bond distance of 1.61 Å, quite consistent with the experimental and theoretical evidence that the ground-state LiOLi molecule is essentially $Li^+O^{-2}Li^+$ in nature near its potential minimum.

3.4.2.2. *The first electronically excited state ($\tilde{A}^1B_1$) of LiOLi.* Breckenridge *et al.* [92] were also able to characterise experimentally the first ($\tilde{A}^1B_1$) singlet excited state of the LiOLi molecule by means of LIF (laser-induced fluorescence) and R2PI (resonance-enhanced two-photon ionisation spectroscopy). This LiOLi excited state was shown [92], in contrast to the ground state, to be strongly bent ($\theta = 105 \pm 5^\circ$) and to have a substantially larger Li–O bond distance of $1.87 \pm 0.04$ Å than the 1.61 Å distance of the ground state. This was attributed to an electronic transition from the '$O^{-2}$' orbital in ground-state $Li^+O^{-2}Li^+$ to a molecular orbital which was Li–Li bonding in nature [92] (consistent with earlier theoretical postulates [93]), thus resulting both in a bent molecule and in less strongly ionic ($Li^{+0.5}O^{-1}Li^{+0.5}$) bonding. This conclusion was consistent with an *ab initio* effective charge distribution [94] calculated for this $^1B_2$ state of $Li^{+0.48}O^{-0.96}Li^{+0.48}$. In fact, it was postulated [92] that this state is (effectively) the $Li_2^+$ ion bound Coulombically to the $O^-$ ion. Thus, both the ground-state and the first excited state of LiOLi are quite ionic in nature.



### 3.5. $M^+M^-$ excited electronic states

Chemists in the past have been trained to think of metal atoms as only electropositive in character, but that is far too simplistic, especially for the heavier transition metal atoms to the right of the 5d row in the periodic table. As a relevant example, the EA of the Au atom is quite highly positive, 223 kJ/mol [54] (2.31 eV), almost as positive as that of the I atom [54]! (in fact, the electronegativities of Au and I are essentially identical [54]). The reason for this strongly positive EA for Au is that the extra electron goes into a 6s orbital, which is strongly stabilised by relativistic effects, since it penetrates well to the highly-charged Au nucleus, and by the lanthanide correction

This raises the unusual possibility that 'ionic' character in diatomic molecules of atoms like gold with other atoms (or molecules) could involve CT *to* the metal atom M, rather than *from* it. Morse *et al.* [95] found that a particular $Au_2$ excited state ($BO_u^+$) had an unexpectedly short radiative lifetime, and postulated that the state had $Au^-Au^+$ electronic character, so that the 'CT' electronic transition to this state was unexpectedly strongly allowed. Simple Coulombic calculations of the $Au^+Au^-$ potential curve from the $Au^+ + Au^-$ asymptote show that it has an energy only slightly higher than that of the short-lived $BO_u^+$ state on its bound outer-limb, consistent with the postulated $Au^+Au^-$ character when smaller ion-induced dipole contributions to the $Au^+Au^-$ bonding are included (Section 3.1). The primary $Au^+Au^-$ nature of the $Au_2(BO_u^+)$ potential curve is consistent with two *ab initio* calculations [96,97] of this unusual electronic state.

## 4. Extension of the harpoon model: reaction dynamics of excited metal atoms, angle-dependent reactions and stereochemistry

The last example on $Au_2$ dimers and that of MgH in Section 2.1 have recalled that in the same molecule covalent and ionic states exist simultaneously. In the latter example, the two ionic and covalent potentials exhibit an avoided crossing at a distance $R_{cross} > R_e$. This description of a one-dimensional crossing has led to the formulation of a model for chemical reactions involving three or more atoms in which the reagents are neutral, for example, $Na + Cl_2$, and the ionic products, $Na^+Cl^- + Cl^\bullet$, the harpoon model [2]. This model is based upon the observation that the cross-section for reaction of alkali atoms and halogen molecules is directly derived from the $R_{cross}$ already alluded to in Section 2.2.2. Hence, the reagents approach along the covalent curve and first feel feeble forces of dispersive or repulsive character, until they cross at $R_{cross}$, the steeply descending $Na^+Cl_2^-$ CT Coulomb potential. At $R_{cross}$, the electron has jumped from the 3s metal orbital (HOMO) to the antibonding $\sigma^*$ orbital (LUMO) on $Cl_2$. There results an avoided crossing between the potentials and then the system continues adiabatically on the ionic potential. The description is that the electron jump has created a force (ionic) that 'harpoons' the reagents together until the newly formed $Cl_2^-$ molecule rapidly dissociates ejecting $Cl^\bullet$, and leaving the $Na^+Cl^-$ product highly excited vibrationally. The probability of switching from the covalent to the ionic potential depends upon the matrix coupling element and in turn on the overlap between the donating and accepting orbitals. This model has been important in molecular reaction dynamics because it determines in simple terms the forces at the TS between a metal and oxidant depending in particular upon the $R_{cross}$ value in the system [98].

In its usual form, the Harpoon model reduces the dynamics of the reaction to a one-dimensional path across the TS of the reaction, where an electron jumps from the metal atom to the molecular reactant generating a one-dimensional approach of the metal and the molecule, then a one-dimensional dissociation occurs on the now repulsive negative ion. The TS is the CT intermediate, $M^+$-Oxidant$^-$. Two different coordinates are at play in the reaction, which do not act simultaneously. This mechanism has been the basis for dynamical studies in triatomic systems [99] and the basis for the classification of reaction dynamics at the TS [3].

### 4.1. *The case of M* + HX(X = halogen) reactions*

In contrast to $M+X_2$ reactions, the reactions with HX are mostly endothermic since the new M–X bond does not compensate for the loss of the strong H–X bond. Therefore, the necessary energy for the reaction has to be sought in translational, vibrational or electronic excitation. The typical example is the reactions of Na with the various HX systems. It has been studied in crossed molecular beams by Lee's group [100,101]. The central outcome is a dramatic enhancement of the reactivity of excited Na $3P_{3/2}$ as compared with ground-state Na $3S_{1/2}$, when above threshold. The product state distribution for the excited state of sodium does not conform well the direct interaction direct repulsion (DIPR) model [102] of electron jump and $HCl^-$ bond dissociation, followed by $Na^+Cl^-$ bond formation. It is argued that the crossing region occurs at ~3.5 Å and thus a certain amount of concertedeness between supposedly independent coordinates, i.e. the reagents approach and the H-Cl recoil, diminishes the validity of the DIPR model. This is a sign that the

reaction occurs on the ground state surface on a late TS involving H–Cl elongation. This is in agreement with the fact that attached electrons can form only a very weak $HCl^-$ molecule at long distance [103], well above the ground $v = 0$ level of HCl. The case of Na $3S + HF$ is even more dramatic since the reaction has a barrier 1.26 eV above the Na + HF asymptote and experimentally the reaction cannot be produced from the ground-state HF reagent. Experiments were carried out in crossed beams [104,105] and within van der Waals complexes after photoexcitation [106]. Both experiments confirm a late barrier associated with a stretch of the HF coordinate. Thus, the excited state reaction from a covalent state correlating with Na $3P_{3/2}$+HF proceeds by surface hopping (through non-adiabatic coupling at the closest approach between surfaces) on a region that is mostly ionic in character, on the ground-state surface [106] (Figure 9).

Here, for the alkali + HX reactions, the main effect of the electronic excitation is to provide the necessary energy to pass over the barrier, but also to allow landing by surface hopping on the appropriate region of the reaction surface in the ground state where the electron transfer can occur. On the other hand, the exploration and excitation of alkali-earth metal reactions with HX yields a much richer panorama than the basic harpoon model. The major advantage of these systems is to populate not only the ground state of the products but also the electronically excited products.



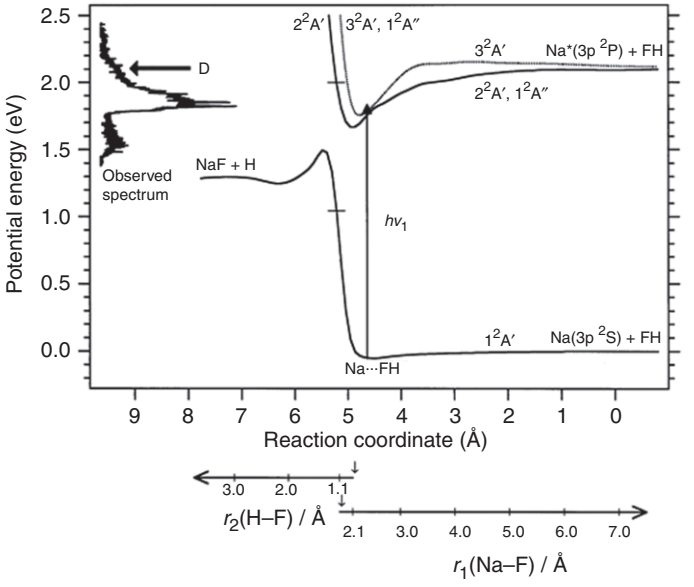


Figure 9. Calculated potential energy curves for the ground and the three lowest electronically excited states, along the approximate minimum energy path of the collinear PES. An upward transition corresponding to typical excitation energy (670 nm; 1.85 eV) is shown.
*Notes:* The action spectrum has been superimposed on the energy axis (the arrow marked. D gives the energy of the D line). In this collinear representation (but only the collinear), the PE curves for the $2^2A'$ and $1^2A''$ states, which for longer Na–F distances represent the two components of the $^2\Pi$ state, and the PE curve for the $3A'$ state, which for longer Na–F distances reduces to the $^2\Sigma^+$ state, cross (adjacent to the $h\nu_1$ arrowhead) The equilibrium values for the Na–F and H–F bond lengths are indicated on their respective axes by two small arrows at $r_{01}$(Na–F) = 1.926 Å and $r_{02}$(H–F) = 0.917 Å [106].

A systematic study of Ca* + HX reactions has also been done in the group of Zare [107] by beam gas methods. In the approach of the reagents, excited metal + oxidant, a series of CT surfaces are crossed which correlate with the ground-state metal ion or *excited states of this ion leading to excited products*. The branching to a surface with an excited metal core leads by conservation of the excited core to excited products (electronic adiabaticity). Thus, the electronically excited products correlate with electronically excited configurations of the metal ion, as described in the ligand-field model of CaX [61]. For example, in the CaCl product the two lowest excited orbitals are two non-bonding $\pi$ and $\sigma$ orbitals which are hybridised 3d$\pi$ and 4p$\pi$ or 3d$\sigma$ and 4p$\sigma$ respectively, in the metal ion [107].

Therefore during the collision process, the access to excited CT curves (Figure 10) correlating with the metal ions in the $^2$D or $^2$P states should yield excited products in either $\Sigma$ or $\Pi$ states. When the Ca4s4p approaches the HCl molecule, if the first crossing has been passed without reaction, the two inner crossings $R_D$, $R_P$ in Figure 10 correspond to an electron jump from the 3s orbital to HX, retaining the 3p orbital on the metal ion and its alignment. Passing trough the inner crossing $R_D$ leads to some preference in the formation of excited states of $\Pi$ or $\Sigma$ symmetry, depending upon the initial alignment of the excited with the future bond axis. An initial symmetry of the collision partners in a metal beam + gas environment can define the initial electronic symmetry of the system in terms of a $\pi$ or $\sigma$ collision depending upon the orientation of the excited atomic orbital with respect to the relative velocity vector between the collision partners. This velocity is essentially collinear with the metal beam direction within the experimental conditions. A parallel alignment of the electric field will lead to a $\sigma$ collision and vice versa.



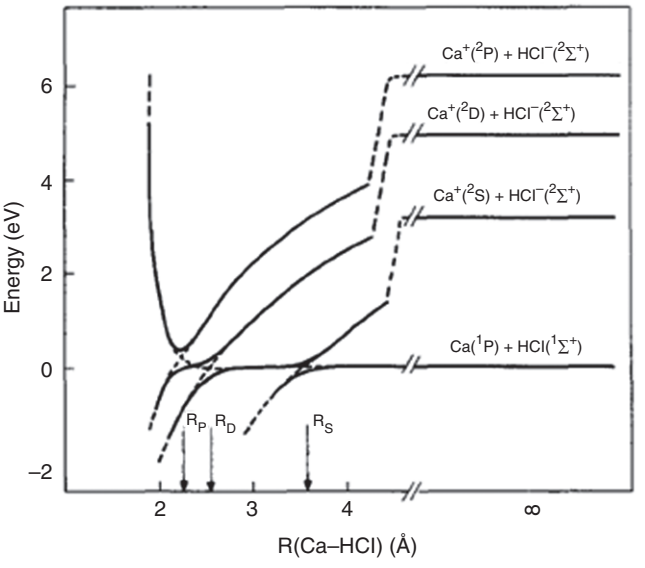


Figure 10. Schematic diagram of the potential curves appropriate to the electron jump model of the $Ca^1P_1 + HCl$ reactions from ref [107]. The covalent surface is crossed by ionic surfaces. These crossings occur at $R_S$, $R_D$ and $R_P$, corresponding to formation of $HCl^-$ with the $^2S$, $^2D$ and $^2P$ states of the $Ca^+$ ion, respectively.

Experimentally, it has been found that for collisions of Ca $^1P + HCl$ in a $\pi$ perpendicular collision arrangement, the A($^2\Pi$) state of CaCl was preferentially formed and B($^2\Sigma$) for a $\sigma$ collision [107]. Also, initial states of $\sigma$ collision symmetry can anticross at the first crossing $R_S$ and draw an important flux to the ground-state product directly, reducing the chemiluminescence efficiency on the CaCl B($^2\Sigma$) state. Although the chemiluminescence yield of the B state is lower than that of the A state, it is not drastically lower, not much more than the statistical ratio between a doubly degenerate $\Pi$ state and a non-degenerate $\Sigma$ state. This indicates the rather high efficiency of the inner crossings producing the chemiluminescence and that this $R_S$ crossing is not dominant, at least for this reaction.

The initial orbital alignment in the collision is difficult to achieve, since for instance, strong intermolecular forces between the reagents can act before the crossing has been reached, hence scrambling the alignment. Also, the above results implicitly suppose orbital following in the collision and do not take into account the reaction geometry, since HCl is randomly oriented with respect to the collision.

The orbital alignment can be best viewed within the molecular frame of the collision complex, where a $\pi$ or $\sigma$ approach for an excited p orbital of the metal correlates with an identified $\Pi$ or $\Sigma$ state of a van der Waals complex formed by the reaction partners and also in a *definite* geometry [109]. These states have spectroscopic characteristics that differentiate them: in general p$\Pi$ states are more attractive than p$\Sigma$ states. The orbital orientation effect has been observed in the reaction of Ca*$\cdots$HBr complexes where there is an important correlation of $\Sigma$,$\Pi$ states of the complex with $\Sigma$,$\Pi$ states of excited CaBr, see Figure 11 and [110]. The main advantage of this approach is that the orbital alignment is uniquely defined by the symmetry of the electronic state of the complex, and in a region



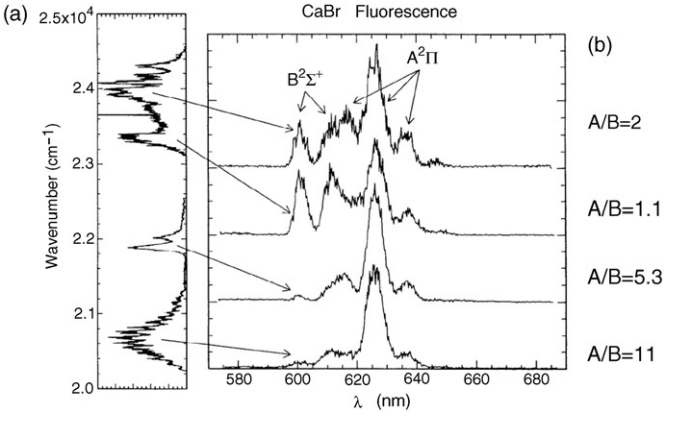


Figure 11. The left panel (a) corresponds to the Ca–HBr action spectrum. In the right panel, (b) the fluorescence spectra corresponding to the four different excitation frequencies of the excitation laser shown by the arrows are presented together with the A/B luminescence ratio derived from Franck Condon simulations of the emission spectra.
*Notes:* The top two emission spectra correlate with the excitation of the Ca4s4p region, while the lower two spectra relate to Ca4s3d. It appears clearly that in the $\Sigma$ regions (for instance at 23,500 $cm^{-1}$), the CaBr $B^2\Sigma$ state is favoured by a factor of 2 over the $\Pi$ region. The $\Sigma$ and $\Pi$ regions of the action spectrum are well separated [108].

of the potential surface next to the transition domain. This is the reason why the branching ratio observed for the CaX excited states with states correlating with $Ca^1P_1$ is much higher in the complex with HBr than it could be in collisions of $Ca^1P_1$ with HBr. This results from (1) the fixed geometry of the complex [109] as compared with collisions, (2) the proximity of the excitation to the transition sate avoiding reorientation of the orbital alignment prior to reaction.

The above experiments have shown that the extension of the harpoon model can rationalise the branching to chemiluminescent states through specific excited CT states between excited metal atoms and the oxidant. This illustrates the general power of this model.

### 4.2. *The angle-dependent harpoon model*

The harpoon model involves a clear dependence on the distance between the reactants to initiate the reaction via an ionic/covalent crossing. When this crossing occurs at long distances, typically much beyond the van der Waals radius of the reagents, the overlap between the donating orbital from the metal and the accepting orbital on the oxidant is poor, but the relative orientation of the reagents is also of minor influence. This stems from the large 'acceptance' angle of the molecule as viewed from the metal atom side. In such a case, the reaction mechanism has been pictured as a stripping process whereby the products, after the capture of the electron, follow in the forward direction irrespective of the reagent orientations. Similarly, a system with a crossing radius at long distances with a ground-state metal atom, is not going to be strongly influenced by the excitation of the metal in terms of increase in cross-section and angle dependency. In reactions of Na 3S or 3P with $Cl_2$, the electronic excitation increases the reactivity, but not as much as the harpoon model cross-section would predict [66].



In turn, for reactions occurring at much shorter distances, a strong angle-dependent effect is at play and has been brought into evidence in the seminal experiments by Brooks [111] for the reaction of $K + CH_3I$. This reaction occurs with a rebound mechanism and the products are deflected backwards. A difference in reactivity is observed when the iodine atom in $CH_3I$ is heading towards the metal atom or the methyl group. The strong angle dependency was interpreted as due to the existence of a cone of acceptance for the reaction, or as a steric hindrance in the case or $Rb + CH_3I$ [112,113]. A polar representation of the reaction probability is given in Figure 12. The reaction mechanism, from the data, involves a cone of non-reaction and is more determined by the steric effect than by the angle dependence in the crossing radius. Systematic exploration of strong angle dependence of the reactivity has been made by the group of Loesch on even larger systems, like $C_6H_5$–I [114]. There a harpoon-type effect is at play with maximum probability in the K–I–$C_6H_5$ alignment. Two effects have been invoked to explain the angle dependence of the steric effect. The partial transfer to the $\pi$ cloud creates an initial repulsion, then the $\sigma^*$ accepting orbital located on the iodine atom causes the bond break, as in the traditional model. The second argument relates to the steric repulsion of the $C_6H_5$ group making difficult the approach to the critical crossing distance, better achieved in the case of a direct attack of the iodine atom by K.

The two effects should simultaneously be at play. In the angle dependence of the reaction of neutrals, many forces are acting already at long distances. Thus if the reaction

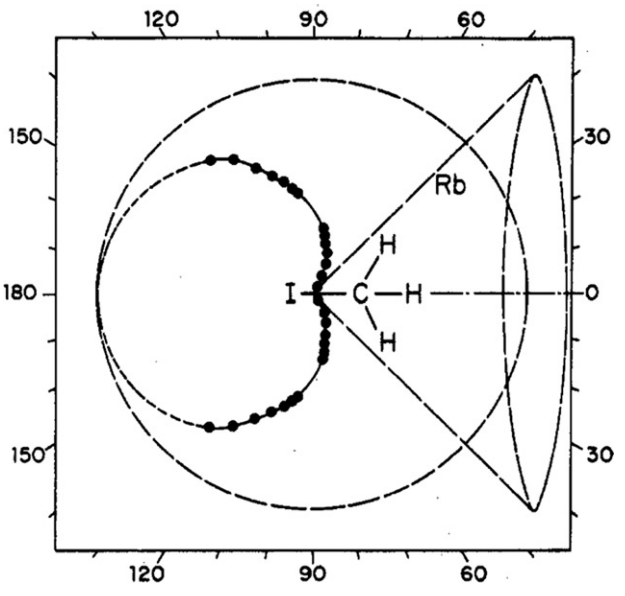


Figure 12. Polar coordinate representation of the observed reaction probability. Radial distance proportional to reaction probability (for centre of mass back-scattering). The angle variable is $\pi-\theta$. The polar plot of c.m. angular distributions of KI product resembles that of the analogous $CH_3I + K$ reaction. (Also shown is a dashed circle representing a hypothetical *isotropic* orientation dependence.) Any approach of Rb within the indicated cone results in no reaction is given in [112] and notes therein.



proceeds at intermediate distances where no selection or repulsion can occur, reorientation forces can mask experimentally the observation of angle-dependent dynamics at the TS level: the reagent molecule is reoriented before acting. This effect has been specifically studied for the Ca $(4s3d^1D_2) + CH_3F$ reaction by changing the collision energy [115]. It was observed that the orientation effect strongly increased with relative collision energy. Thus, rapid collisions did not allow time for reorientation to favourable or unfavourable angles to the reaction. Also, the angle-dependent barrier separating the favourable and unfavourable configurations is in this case rather high, otherwise the collision energy increase would have made favourable all angles [115].

In the case of the intracluster reaction, $Ca(^1P)\cdots HBr$ already detailed in Section 4.1, the excitation region of the reaction reflects in a spectroscopic manner the potential energy surface in the transition region which can be directly mapped. Thus, by numerical propagation of a wavepacket projected by a white light pulse on the excited surface, here the PΠ branch, it is possible to reproduce the experimental spectrum using a model of two-dimensional potential energy surface. The modelling reproduces the position of the bands in the spectrum as well as the widths, revealing the dynamics on the surface. With the help of this model, it was possible to deduce that the reaction occurred in a bent $Ca\cdots HCl$ geometry near 90° in a rather small acceptance angle [116]. Such an angle-dependent harpooning is caused here by an optimum overlap in the broadside geometry, of the diffuse Ca(4s) donating orbital with the antibonding $\sigma^*$ accepting orbital located on the H atom of HCl. This Ca(4s) orbital has been tracked as the donating orbital in Section 4.1 by

the 'conservation' of the Π electronic symmetry over the course of the reaction, only possible if the electron has jumped from the 4s orbital.

Thus, we have seen that modifications can be brought into the harpoon model taking into account the deeper reality of the collision encounter, without any loss of generality.

## 5. Dynamics of excited metal atom/molecule systems where the molecule has a negative EA

### 5.1. *Relaxation dynamics of excited metal atoms*

Like the $O^-$ ion (Section 3.4.2), many diatomic molecules like $N_2$, CO and $H_2$ have negative vertical EAs, but it was postulated early on [117,118] that the unstable diatomic molecular ions could be stabilised by Coulomb attraction to metal ions $M^+$, where the metal atom M has a low IE. Such $M^+/(\text{diatomic})^-$ potential surfaces, it was thought, could especially cross the asymptotic potential surfaces of high-energy excited state (M* + diatomic) potential surfaces at long range, and in fact this was originally thought to provide 'intermediate' potential surface crossing mechanisms by which some excited M* states were deactivated relatively efficiently to the ground-state M atom (plus vibrationally excited ground-state molecules). This 'Fischer–Bauer–Gilmore' (FBG) model [117,118] for the quenching of M* states by diatomic molecules was attractive in its simplicity, but was of course in no way sufficiently sophisticated to describe the detailed dynamical processes involving complicated excited and ground-state triatomic potential surfaces. There was also the difficulty of estimating the negative EAs. However, in an earlier review of quenching of excited metal atoms, Breckenridge and Umemoto [119] showed that the FBG model was remarkably consistent for several classes of molecules in predicting whether the quenching cross-sections were qualitatively large (facile $M^+$-$Mol^-$/M*-Mol curve crossings) or unexpectedly small. The exceptions [119] for large cross-sections usually involved specific chemical interactions (for example, the efficient chemical reaction of $Mg(3s3p\,^1P_1)$ with C–H bonds in alkane hydrocarbons). There were essentially no exceptions for any 'predicted' large cross-sections turning out to be small. This at least indicated the possibility [119] of CT character in the adiabatic excited-state potential surface being important in many excited metal atom quenching process by small molecules with negative EAs.

Later experiments and theoretical treatments [120] showed that the FBG model, as expected, was too simplistic. For example, although the 'vertical' EAs of diatomic molecules like $H_2$, $N_2$ and CO are negative, it is now known that these molecules can accept an electron favourably, if the bond length is slightly increased: that is, the $N_2^-$, $CO^-$ and $H_2^-$ ions are actually stable, but $R_e$ values are larger than the neutral molecules [121]. In other words, the 'adiabatic' EAs of these molecules are positive. This means that the M*/diatomic potential surfaces could have $M^+/(\text{diatomic})^-$-type character, if the diatomic molecule bond length increases during the M*/diatomic collisional interaction.

Homonuclear diatomic molecules like $N_2$ and $H_2$ have low-lying, empty, symmetric antibonding orbitals ($\pi^*$ for $N_2$, $\sigma^*$ for $H_2$) which can readily accept electron density from M(np$\pi$) excited atomic orbitals when the diatomic molecule is perpendicular to the bond axis ($B_2$ symmetry in $C_{2v}$). This can result in moderately attractive M*(np)–diatomic potential surfaces, with the antibonding component of the bonding resulting in 'stretching'

of the diatomic molecule [121]. The attractive M*(np)–diatomic potential surface can thus cross the repulsive M(ns)–diatomic ground-state surface, resulting in efficient electronic quenching, forming vibrationally excited diatomic molecules and ground-state M(ns) atoms [121].

The question, then, is how much $M^+$–(diatomic)$^-$ character is there in these excited state surfaces, and even if there is some, is there a 'sudden' harpoon-like region of the M*(np)–diatomic potential surface in which $M^+$/(diatomic)$^-$ character rapidly appears (that is, something akin to, but more complicated than, what was postulated for the FBG model)?

The answer, from several *ab initio* calculations [121], appears to be 'no': there is no 'sudden' diabatic appearance of $M^+$(diatomic)$^-$ character in the M*(diatomic) potential surface as was postulated in the original FBG model, but rather a smooth adiabatic decrease in potential energy in the attractive $B_2$ potential surfaces as the M*(np$\pi$ state approaches the diatomic molecule, with a concomitant 'stretching' of the diatomic bond length [121]. There is increasing ionic character in the bonding, for sure, as the M*(np$\pi$) orbital donates electron density into the empty diatomic anti-bonding orbitals, but there is no *ab initio* evidence for a 'harpoon'-type completely ionic $M^+$(diatomic)$^-$ intermediate.

The situation for the M*/CO interaction, even though CO is isoelectronic with $N_2$, is more complicated, and interestingly different. From *ab initio* calculations, the Na($^2$P)–CO and Na($^2$P)–OC geometrics are favoured, not 'side-on' geometries [121]. Unlike the homonuclear $N_2$ and $H_2$ empty antibonding orbitals, which are symmetric with respect to each atom, the $\pi$ empty orbital on CO is strongly skewed towards the least electronegative atom, carbon. Thus, an M*(2p$\pi$)–C–O linear approach apparently provides the best geometry for efficient M*(2p$\pi$) donation (similar to M(d$\pi$)–C–O 'back-bonding' in $M(CO)_n$ transition-metal complexes). But the M*(2p$\pi$)–O–C ('isocarbonyl') linear approach is also favourable. This appears to be due to a very large avoided crossing with a much higher energy asymptotic MO of $\pi$ symmetry which is 'essentially' $M^+(OC)^-$ in character, where the negative charge probably resides mostly on the more electronegative oxygen atom. But in both the favourable M*–C–O and M*–O–C linear approaches, the CO bond stretches smoothly, with no evidence of a 'sudden' change to ionic character, which is consistent with the M*/$N_2$, M*/$H_2$ side-on 'bond-stretch-attraction' ideas as discussed above.

To make a complicated story short, then, the simple FBG 'ionic intermediate' model is incorrect, but the M*(p$\pi$ interactions with $H_2$, $N_2$ and CO do result in substantial CT at their potential-energy minima.

### 5.2. *Extension of the harpoon from a one-dimensional to a multidimensional model*

As discussed above, the usual form of the harpoon model reduces the dynamics of the reaction to a one-dimensional path across the TS of the reaction. Two different coordinates are at play in the reaction, which do not act simultaneously. In the last section, the influence of CT on the relaxation of excited atoms by diatomic molecules has been reviewed and we show here how important the elongated bond model discussed in Section 5.1 is for the harpoon mechanism involving polyatomic systems.

Typically, intracluster reactions have allowed the investigation of short-lived excited metal atoms interacting with molecules, resulting in a detailed exploration of the

transition region [122,123]. Several reactions that are not in principle open to the normal harpoon mechanism have shown the same type of dynamics: a direct reaction with high vibrational energy disposal in the fragments. The direct application of the simple model was not possible since the EA of the oxidant was highly negative by several electron volts (HF, $CH_3F$), making the existence of stable or stabilised negative ions unrealistic, even in the field of a positive metal ion. It has been proposed for reactive encounters, as in the preceding section, to extend this model by supposing the existence of an extra coordinate that would lead to a positive EA (Section 5.1). Indeed, when stretched and almost broken in the presence of the metal, the HF coordinate can yield a 'stable' $H \cdots F^-$ with a positive EA at the energetic price of the bond stretch [124], since the F atom has a high, 3.4 eV EA [125]. This, at the TS level makes at least two coordinates active simultaneously: the HF bond stretch and the reactants approach coordinate. Such a mechanism is needed since the reaction products are highly ionic and the reactants, neutral, so that the transition region must allow the charge rearrangement necessary for the reaction to occur.

Representative examples of this effect are found in the $Li^* \cdots HF$ and $Li^* \cdots CH_3F$ photo-induced reactions, reported by the group of Polanyi [126] and the $Ba \cdots CH_3F$ reaction studied extensively in the groups of Gonalez–Ureña [127] and Radloff [128]. In the molecular reactants, C–F or H–F bonds need to be stretched for the attachment of an extra electron on the fluorine. The intracluster reaction

$$Ca \cdots CH_3F \xrightarrow{h\nu} CaF^* + CH_3$$

follows the same trend. It can be considered as prototypical of situations that are not adequately described by the conventional harpoon mechanism, and gives some clues for its extension. The above reaction has been studied in [129–131] and shows a high vibrational energy disposal in the electronically excited states of the CaF product. The action spectrum of this complex has been analysed in light of quantum calculations. The observed bands correlate with the asymptotic excitation of calcium $^1P_1$ or $^1D_2$ [132]. A portion of the action spectrum is displayed in Figure 13, which shows results for the free $Ca \cdots CH_3F$ complex and the same binary complex deposited at the surface of large argon cluster. Three bands appear both in the free complex and the deposited spectra. They are marked by dashed lines, at 24,760, 25,710 and 26,580 $cm^{-1}$ in the free complex spectrum and blue shifted by 200 $cm^{-1}$ in the deposited spectrum. Their positions in the free complex have been fitted with a vibrational progression for vibrational levels $v = 2, 3, 4$ with $\omega e = 1120\,cm^{-1}$ and $\omega exe = 60\,cm^{-1}$ with an origin at 22,400 $cm^{-1}$ These values are very close to the calculations, when assigning the vibrational origin as the calculated (4s4p $^1P$)'$\Pi$' potential, as in Figure 13(b). This reaction mechanism goes through the direct excitation of the C–F stretch within the $Ca \cdots CH_3F$ electronically excited state *that has no electron transfer character*, even less than in the ground state of the complex, since the static dipole moment associated with the state (4s4p $^1P$)'$\Pi$' is smaller than that of the ground-state ($4s^2\,^1S$)'$\Sigma$'. This suggests that solvation by the argon environment should more effectively stabilise the ground state of the complex than this excited $\Pi$ state. This is verified in the action spectrum blue shifted in the argon environment, as shown in Figure 13(a).

The observation of the vibrational progression in this action spectrum is the spectroscopic signature of the activity of this coordinate along the reaction evolution.

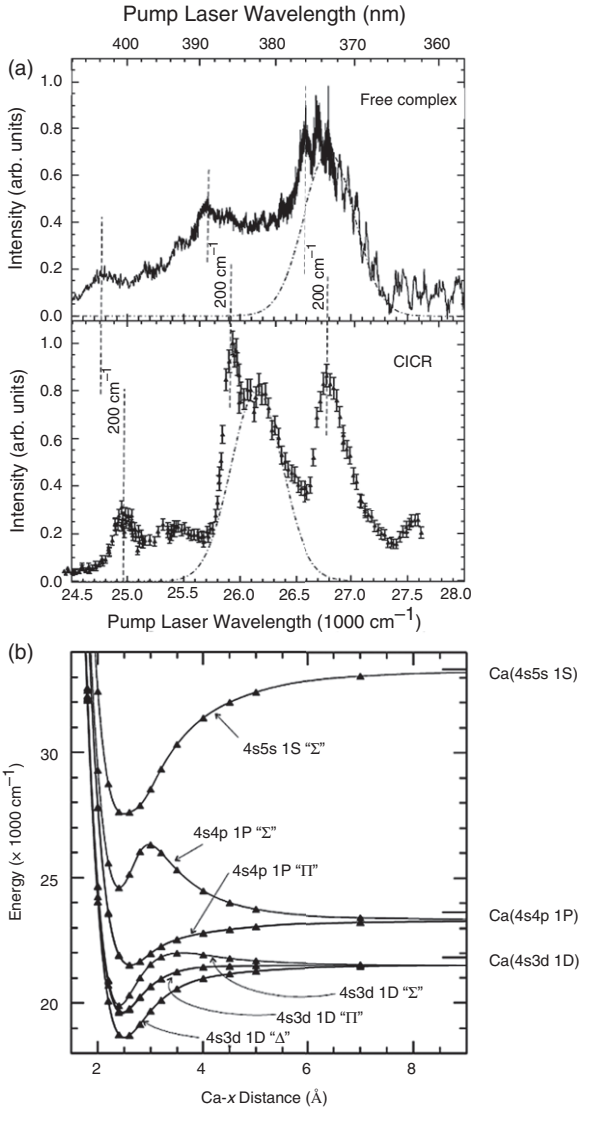


Figure 13. (a) Band B of the action spectrum. The bottom panel recalls the action spectrum measured in a previous experiment where the $Ca\cdots CH_3F$ complex is deposited at the surface of a large argon cluster and CaF(A,B) monitored by its fluorescence (CICR) [130]. (b) Excited singlet state calculation at the RSPT2 level as a function of the Ca–X distance. The labels giving asymptotic energy levels are placed at their experimental values. Figures taken from ref [133].

The coordinate is slightly elongated in the Franck Condon region and the system follows the gradient along this coordinate leading to the CT region. This is one of the rare instances where a moderately bound van der Waals complex ($1500\,cm^{-1}$) so greatly affects the electronic structure of the complexing molecule that one of its vibrations appears in a progression.

Although a quantitative Franck–Condon treatment of the intensity of the bands is still difficult, the first signature of the involvement of the C–F stretch has been found as the promoter of the harpoon mechanism.

## 6. CT in excited states of large molecules containing metal atoms

In large systems containing metal atoms and organic molecules, the CT states are located at rather high energies as compared to their ground state. Thus, if not accessed directly by optical excitation, they can be reached via excitation of higher excited states. The presence of metal atoms in the structure will bring these states to lower energy regions. These CT states are in general rather elusive since their charge distribution differs from that of all valence states and for this reason might be difficult to access optically. For this same reason, since they have different configurations from valence states, they can connect electronic states of very different configurations and serve as doorways to the relaxation of electronic energy. The case of metal atoms embedded in molecular assemblies using this mechanism is exceedingly interesting since the CT properties control essential processes in living systems such as photosynthesis, so that their study at the molecular level is important.

Here we shall describe how CT states are essential in connecting two classes of states in MP. MP are composed of a conjugated ring hosting in their centre a metal (Figure 14). The electronic states of the conjugated ring are distinct from that of the metal. The CT states possess different properties from the others, ring centred or metal atom centred. However here, the metal, in contrast to the preceding cases of this review, is bound either in a suitable molecular cavity or by ligands or both (Figure 14). In MP, the metal atom is in the oxidation state II or III, which corresponds to formally positive charges on the metal and negative charges on the porphyrin ring. In fact, in the ground-state the Mulliken charge distribution on the metal is usually close to zero [133]. The metal can be either an acceptor or a donor, and this represents the specific property of transition metal porphyrins (TMP)



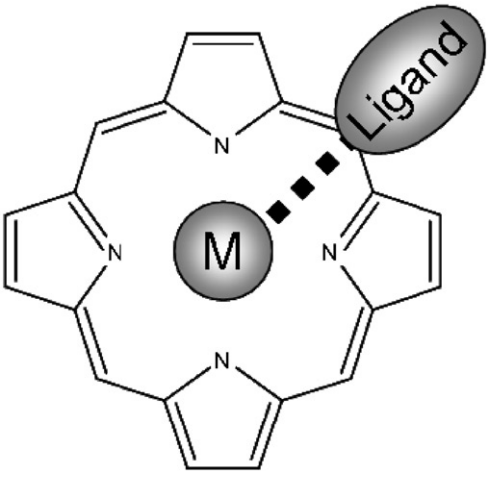


Figure 14. Schematic representation of a ligated metalloporphyrin.

which results from the quasi-equivalent ionisation potential and EA for the metal and porphyrin moieties. It is in fact the complex interplay between the metal and the ring that controls the electron attraction or donation properties, or redox properties, of the metal. In turn when a ligand is attached to the metal, it senses directly the electron density at the metal atom as the metal–ligand bond is due to partial charge donation from the ligand to the metal. As an example, the iron in haeme when in the oxidation state II can ligate oxygen and cannot in oxidation state III.

As mentioned, we wish to focus on another important aspect here, the role of CT states in the electronic relaxation of TMP. These CT state are essential relay states in the relaxation of MP. In these molecules, there are electronic states localised on the porphyrin ring (the optically active states), states localised on the metal (inactive) and CT states. These latter states channel the excitation from the porphyrin to the metal and eventually vice versa if a triplet state of the porphyrin can be accessed. As an example, the electronic states of nickel porphyrin have been calculated by time-dependent DFT [134] and there are three CT singlet states between the two excited $\pi\pi^*$ transitions involving the porphyrin. One notes that many excited states belong to two categories either porphyrin to metal CT or the reverse, porphyrin to metal.

The characterisation of these states is a difficult task experimentally (and even more theoretically), given the size of these systems and the nature of the states. In this respect, the best comparison between theory and experiment should be done with gas phase results, in the absence of solvation, as presently most of the experiments have been conducted in the condensed phase by transient absorption spectroscopy or *excited state* Resonant Raman Spectroscopy to characterise the transient electronic states [135,136].



In the following, we discuss a scheme for the relaxation of the $S_2$ state of several MP in the gas phase and its importance. The initial state $S_2$ is the $(\pi\pi^*)$ $(a_{1u},e_g)$ (in $D_{4h}$ symmetry) state accessed by the Soret band at 400 nm [137]. $S_1$ and $S_2$ excitations are both centred on the porphyrin ring as represented in Figure 15. The subsequent evolution from the $S_2$ state has been analysed in [138] and is summarised in Table 7. It shows a striking difference when the metal belongs to group IIb, that is, a d-filled shell metal or a transition metal. In the first case, a classical $S_2$–$S_1$ electronic relaxation is observed with a decay constant of 600 fs, followed by fluorescence emission from the $S_1$ state. On the other hand, in a porphyrin containing a transition metal, this latter atom offers a convenient trap for the delocalised electron of the excited porphyrin and provides a rapid sink for the excitation. For all transition metals, the decay occurs over the first 100 fs and the excitation remains trapped on the metal. These steps of the decay are described in a model following Gouterman [137] and the results of Zewail *et al.* [139]. The initial step in the relaxation leads to a porphyrin-to-metal charge ($\bar{e}$) transfer, CT, followed by retro-donation to the porphyrin from a low d orbital of the metal to the ring, thus preparing a $(d, d^*)$ state localised on the metal as described by steps 2 and 3 in Figure 15. Substitution on the porphyrin ring (TPP or OEP) thus has only a small effect on the values of the decay constant, $\tau_1$. This relaxation scheme of $S_2$ involving the metal to porphyrin CT state is fully supported by the dependence of the relaxation upon the nature of the metal-filled d shell of the transition metal, making this transfer possible. On the other hand, the ionisation of the MPs draws an electron from the porphyrin, not from the metal, which rationalises the electron jump from the porphyrin to the metal.

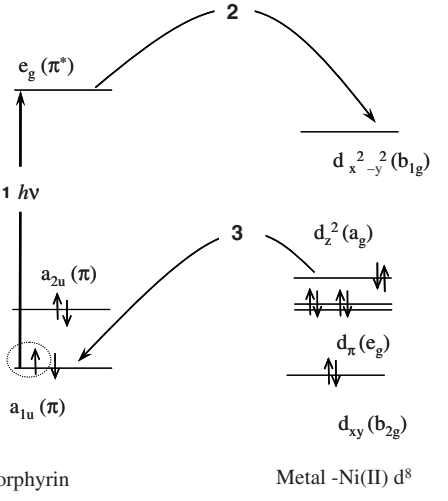


Figure 15. Energy levels of separated TPP and Ni metal orbitals in the ligand-field approximation. This scheme describes the initial steps of the relaxation pathway of the $S_2$ excited state. (1) Excitation, (2) Ultrafast CT from the porphyrin ring to the d orbital of the metal, likely via a conical intersection. This decay is followed at longer times by (3), a back transfer from the metal to the half empty porphyrin orbital $a_{1u}$.



Table 7. Initial decay lifetimes and properties of the $S_2$ excited state of different MP: M-TPP or M-OEP.

| Metalloporphyrin | Configuration of the metal | Lifetime of initial state $S_2$ (fs) | Lifetime of relaxed state | $\sigma_2/\sigma_1$ |
|---|---|---|---|---|
| Zn TPP | D10 | $600 \pm 50$ | 3 ns | $1.0 \pm 0.1$ |
| FeIII OEP | D5 | $50 \pm 10$ | $2000 \pm 100$ fs | $0.33 \pm 0.05$ |
| RuII OEP | D6 | $80 \pm 10$ | $1200 \pm 100$ fs | $0.33 \pm 0.05$ |
| RuII TPP | D6 | $70 \pm 10$ | $1200 \pm 100$ fs | $0.33 \pm 0.05$ |
| CoII TPP | D7 | $70 \pm 10$ | $500 \pm 100$ fs | $0.11 \pm 0.05$ |
| NiII TPP | D8 | $50 \pm 10$ | $375 \pm 25$ fs | $0.20 \pm 0.02$ |
| NiII OEP | D8 | $100 \pm 10$ | $1200 \pm 100$ fs | $0.25 \pm 0.02$ |
| CuII TPP | D9 | $65 \pm 10$ | $2000 \pm 100$ fs | $0.075 \pm 0.025$ |
| CuII OEP | D9 | $65 \pm 10$ | $2000 \pm 100$ fs | $0.25 \pm 0.02$ |

The results indicate that the TMP listed in Table 7 behave in a similar manner. Therefore, there must exist a suitable accepting orbital for all TMP. A possible orbital candidate to accept the charge from the porphyrin macrocycle is the $d_{x^2-y^2}$ orbital of the central transition metal, with $b_{1g}$ symmetry for Ni through Cu. This orbital is the highest in energy for all metals owing to its interaction with the porphyrin within the plane of the molecule, thus this $d_{x^2-y^2}$ orbital is vacant for all metals studied in this work, except for Zinc. However, the calculations of Liao *et al.* [140] show that it could be slightly too high in energy for FeII and CoII. For these metals, the lowest unoccupied orbital LUMO of the metal is $d_z^2$ which has thus been inferred to serve as the mediating orbital by Zewail *et al.* [139] for CoTPP.

The very rapid initial relaxation decay, <100 fs from the $S_2$ excited state points to a direct descent on a potential energy surface that connects the two electronic states via a conical intersection, between the $S_2$ ($a_{1u}$,$e_g$) state and the CT state of $B_{1g}$ symmetry in point group $D_{4h}$. It has been proposed in [138] that the mediating coordinate could be found in the doubly degenerate $e_{1g}$ modes of the pyrolle subunits. These modes involve a motion of the core suitable to couple the $\pi$ electronic cloud of the porphyrin and the $d_{x^2-y^2}$ orbital of the metal. These vibrations have also a suitably fast (40 fs) period to involve a quick departure of the initial wavepacket from the initial geometry. This vertically accessed geometry is likely to be close to planar, as are the ground state, $\pi^2$, porphyrins. The same arguments will hold, involving the doming motion and a pyrolle deformation in CoTPP where the $d_z^2$ ($A_{1g}$) orbital is involved. This CT state can undergo back CT from one low-lying d orbital to the empty $a_{1u}$, $\pi$ orbital as shown in Figure 15. The resulting state is excited on the metal (d, d*) and this agrees with the observations of Holten [141] and Mizutani [142] from excited-state resonant Raman spectroscopy.

It was also observed that the ligated ruthenium porphyrin RuPorphyrin–CO [138] exhibits a rapid initial decay and this can also be interpreted in light of the preceding ring to metal CT mechanism. After the 70 fs electronic relaxation, the CT to the ruthenium core destabilises the Ru–CO bond, constructed upon electron donation from CO (and back donation from Ru). The CO is ejected as soon as the wavepacket reaches the relaxed surface, then the decay of the parent corresponds to the electronic relaxation to the CT state.

It is seen here that CT states play a mediating role in the system combining two distinct entities, the porphyrin and its metal host. The porphyrin collects the light and the excitation can be transferred to the inactive metal atom via these CT states. This is in marked difference with usual metal carbonyl compounds where the most intense transition is a CT one [143,144], directly accessed by absorption of light. The cascade of states which are populated during electronic relaxation depends on the d orbital filling of the central metal atom. Thus, whether zinc or a transition metal atom is at the centre of the porphyrin pocket, the electronic relaxation properties are profoundly modified depending upon the fact that CT sates can be involved or not.



## 7. Conclusions

We have examined here with the eyes of experimentalists the specifics of ionic chemical bonds in molecules containing a metal atom or reactions involving CT intermediate states. This choice results from the generally low ionisation potential of metal atoms which places these systems as models of ionic bonds and of their unavoidable mixed ionic covalent character at some level or another. The large body of experimental evidence allows the description of the ionic bonds in an empirical way or a semi-empirical way ranging from partial point charges to polarised charges. This is done by comparing with more quantitative models, to put on firmer grounds simple descriptions of ionic bonds which are often obscured somehow in quantum chemical analysis.

The fundamental aspect of these metallic systems is the fact that they dissociate into neutral atoms and molecules, and that there is thus an adiabatic passage through a mixed ionic covalent region of the potential surface. This is well-known and can be accounted for qualitatively by a crossing between a CT potential and a neutral potential. In simple systems such as MgH, quantum chemistry calculations reproduce well this behaviour in

several excited states. In an already more complex triatomic system, neutral Mg + OH fragments lead after a conical intersection to a bent $Mg^+OH^-$ molecule. In larger systems, exploring the CT PES is at the limit of calculation possibilities owing to diffuse orbitals. These difficulties already appear in excited states of these molecules (MgOH) where convergence is difficult to achieve. Owing to the fact that the potential attraction of the bent ground-state $Mg^+OH^-$ can be reproduced with a simple CT potential, this validates the use of empirical and semi-empirical models to tackle more difficult systems impossible to quantitatively describe by quantum chemistry calculations.

Accordingly, the harpoon model describing reactions of metals with oxidants via a CT curve crossing can be extended from a one-dimensional path to a multidimensional path and from a single electron jump to a more elaborate multielectron rearrangement, integrating thus the results of widely varied experimental systems.

The question remains: which new experimental methods can tackle directly the partial ionic character of bonds since the quantitative description by quantum chemistry has its limits for excited systems or larger than triatomics systems? All methods reported here are indirect, since none of the observables examined directly represent the ionic character of a potential energy surface. For example, the dipole moment is related to charge distribution in an overall way and does not directly account for a partially ionic bond. New approaches applied to very simple molecules, $N_2$[145], $CO_2$[146] namely molecular orbital tomography, endeavour to reconstruct the electronic wavefunction of the HOMO orbital of these systems. It can also be foreseen that visualising the time-dependent evolution of these orbitals as well as that of the HOMO-1 can relate directly to the true representation of CT states. In the same way, attosecond time-dependent electronic wavepacket evolution such as those depicted by Levine and Remacle [147] can render the true nature of the time evolution in these systems by showing the time-dependent amplitude of each of these specific configurations. Lastly, the investigated metal systems relate almost exclusively to alkali, alkali-earths or group IIB metals but more seldom to transition metals. Owing to the richness of electronic configurations in these metals, the detailed exploration of their CT properties should be of the highest relevance since their CT states relate directly to the d orbital occupancy. Practically, these properties rule their behaviour towards oxidation–reduction, as for example, excited states of MP can be either metal to porphyrin CT or the reverse.



## Acknowledgements

W.H. Breckenridge would like to acknowledge his colleagues Jack Simons and Joel Miller for useful discussions, and the Department of Chemistry, University of Utah, for travel grants to support the collaborations with his French co-authors. N. Shafizadeh acknowledges the financial support of Centre National de la Recherche Scientifique through an 'Action Incitative'.

## References

[1] M. Polanyi, *Atomic Reactions* (Williams & Northgate, London, 1932).
[2] J. L. Magee, J. Chem. Phys. **8**, 687 (1940).
[3] J. C. Polanyi, Acc. Chem. Res. **5**, 161 (1972).
[4] P. Linus, *The Chemical Bond* (Cornell University Press, Cornell Ithaca, 1967).

[5] S. Raouafi, G. H. Jeung, and C. Jungen, J. Chem. Phys. **115**, 7450 (2001).
[6] K. Eller and H. Schwarz, Chem. Rev. **91**, 1121 (1991).
[7] M. L. Chabinyc, S. L. Craig, C. K. Regan, and J. I. Brauman, Science **279**, 1882 (1998).
[8] J. Mikosch, S. Trippel, C. Eichhorn, R. Otto, U. Lourderaj, J. X. Zhang, W. L. Hase, M. Weidemuller, and R. Wester, Science **319**, 183 (2008).
[9] D. R. Herschbach (Nobel lecture. 1986) <http://nobelprize.org/nobel_prizes/chemistry/laureates/1986/herschbach-lecture.html>
[10] J. M. Mestdagh, B. Soep, M. A. Gaveau, and J. P. Visticot, Int. Rev. Phys. Chem. **22**, 285 (2003).
[11] J. M. Berg, J. L. Tymoczko, and L. Stryer, *Biochemistry*, 5th ed. (W. H. Freeman & Co, New York, 2002).
[12] D. C. Clary, Proc. Natl. Acad. Sci. USA **105**, 12649 (2008).
[13] F. F. Crim, Proc. Natl. Acad. Sci. USA **105**, 12647 (2008).
[14] C. E. Moore, *Atomic Energy Levels,* Circular 467 (NBS, US Dept. of Commerce, 1949), Vol. I.
[15] D. B. Kinghom and L. Adamowicz, J. Chem. Phys. **106**, 4589 (1997).
[16] A. Shayesteh, R. D. E. Henderson, R. J. Le Roy, and P. F. Bernath, J. Phys. Chem. A **111**, 12495 (2007).
[17] P. Durand and J. C. Barthelat, Theoret. Chim. Acta **38**, 283 (1975).
[18] J.-M. Mestdagh, P. de Pujo, B. Soep and F. Spiegelman, Chem. Phys. Lett. (in press) 2009.
[19] P. E. M. Siegbahn, Theor. Chim. Acta **86**, 219 (1993).
[20] J. Pitarch-Ruiz, J. Sanchez-Marin, A. M. Velasco, and I. Martin, J. Chem. Phys. **129**, 054310 (2008).
[21] T. Leininger and G. H. Jeung, J. Chem. Phys. **103**, 3942 (1995).
[22] I. S. K. Kerkines and A. Mavridis, J. Phys. Chem. A **111**, 371 (2007).
[23] A. Boutalib, J. P. Daudey, and M. Elmouhtadi, Chem. Phys. **167**, 111 (1992).
[24] T. Leininger and G. H. Jeung, Phys. Rev. A **49**, 2415 (1994).
[25] J. Verges, C. Effantin, A. Bernard, A. Topouzkhanian, A. R. Allouche, J. d'Incan, and R. F. Barrow, J. Phys. B Atom. Mol. Phys. **26**, 279 (1993).
[26] F. X. Gadea and T. Leininger, Theor. Chem. Acc. **116**, 566 (2006).
[27] N. Khelifi, J. Russ. Laser Res. **29**, 274 (2008).
[28] N. Khelifi, B. Oujia, and F. X. Gadea, J. Russ. Laser Res. **27**, 575 (2006).
[29] N. Khelifi, B. Oujia, and F. X. Gadea, J. Phys. Chem. Ref. Data **36**, 191 (2007).
[30] N. Khelifi, W. Zrafi, B. Oujia, and F. X. Gadea, Phys. Rev. A **65**, 042513 (2002).
[31] W. Zrafi, B. Oujia, and F. X. Gadea, J. Phys. B Atom. Mol. Opt. Phys. **39**, 3815 (2006).
[32] W. Zrafi, B. Oujia, and F. X. Gadea, J. Phys. B Atom. Mol. Opt. Phys. **39**, 4341 (2006).
[33] A. A. Christodoulides, D. L. McCorkle, and L. G. Christophorou, in *Electron-molecule Interactions and Their Applications*, edited by L. G. Christophorou (Academic Press, London, 1984), Vol. 2, p. 424.
[34] E. Miliordos, A. Papakondylis, A. A. Tsekouras, and A. Mavridis, J. Phys. Chem. A **111**, 10002 (2007).
[35] G. Theodorakopoulos, I. D. Petsalakis, and I. P. Hamilton, J. Chem. Phys. **111**, 10484 (1999).
[36] T. C. Steimle, Int. Rev. Phys. Chem. **19**, 455 (2000).
[37] H. K. Hughes, Phys. Rev. **72**, 614 (1947).
[38] M. Broyer, R. Antoine, I. Compagnon, D. Rayane, and P. Dugourd, Phys. Scr. **76**, C135 (2007).
[39] P. Dugourd, R. Antoine, D. Rayane, E. Benichou, and M. Broyer, Phys. Rev. A **62**, 011201 (2000).
[40] A. C. Legon, Chem. Soc. Rev. **19**, 197 (1990).
[41] C. H. Townes and B. P. Dailey, J. Chem. Phys. **17**, 782 (1949).
[42] J. Maya and P. Davidovi, J. Chem. Phys. **59**, 3143 (1973).
[43] T. Forster, Zeitschrift Fur Elektrochemie **54**, 531 (1950).
[44] O. Cheshnovsky and S. Leutwyler, J. Chem. Phys. **88**, 4127 (1988).

[45] R. Knochenmuss and I. Fischer, Int. J. Mass Spectrom. **220**, 343 (2002).
[46] M. Saes, C. Bressler, R. Abela, D. Grolimund, S. L. Johnson, P. A. Heimann, and M. Chergui, Phys. Rev. Lett. **90**, 047403 (2003).
[47] D. H. Oh, M. Sano, and S. G. Boxer, J. Am. Chem. Soc. **113**, 6880 (1991).
[48] X. Liu, R. L. Gross, and A. G. Suits, Science **294**, 2527 (2001).
[49] A. V. Baklanov, L. M. C. Janssen, D. H. Parker, L. Poisson, B. Soep, J.-M. Mestdagh, and O. Gobert, J. Chem. Phys. **129**, 214306 (2008).
[50] D. E. Folmer, E. S. Wisniewski, and A. W. Castleman Jr, Chem. Phys. Lett. **318**, 637 (2000).
[51] M. Tsubouchi and T. Suzuki, J. Phys. Chem. A **107**, 10897 (2003).
[52] S. T. Pratt, E. F. McCormack, J. L. Dehmer, and P. M. Dehmer, Phys. Rev. Lett. **68**, 584 (1992).
[53] A. G. Suits and J. W. Hepburn, Annu. Rev. Phys. Chem. **57**, 431 (2006).
[54] D. W. Oxtoby, H. P. Gillis, and N. N. Nachtriel, *Principles of Modern Chemistry*, 5th ed. (Thomson Brooks/Cole, Belmont, 2002).
[55] E. S. Rittner, J. Chem. Phys. **19**, 1030 (1951).
[56] M. Shapiro and P. Brumer, Rep. Progr. Phys. **66**, 859 (2003).
[57] M. Kumar and J. Shanker, J. Chem. Phys. **96**, 5289 (1992).
[58] W. J. Childs, L. S. Goodman, U. Nielsen, and V. Pfeufer, J. Chem. Phys. **80**, 2283 (1984).
[59] T. Törring, W. E. Ernst, and S. Kindt, J. Chem. Phys. **81**, 4614 (1984).
[60] T. Törring, W. E. Ernst, and J. Kandler, J. Chem. Phys. **90**, 4927 (1989).
[61] S. F. Rice, H. Martin, and R. W. Field, J. Chem. Phys. **82**, 5023 (1985).
[62] N. Honjou, G. F. Adams, and D. R. Yarkony, J. Chem. Phys. **79**, 4376 (1983).
[63] P. F. Bernath, B. Pinchemel, and R. W. Field, J. Chem. Phys. **74**, 5508 (1981).
[64] H. Hotop and W. C. Lineberger, J. Phys. Chem. Ref. Data **14**, 731 (1985).
[65] R. W. Field and C. M. Gittins, J. Chem. Phys. **106**, 10379 (1997).
[66] P. S. Weiss, J. M. Mestdagh, H. Schmidt, M. H. Covinsky, and Y. T. Lee, J. Phys. Chem. **95**, 3005 (1991).
[67] C. W. Bauschlicher, S. R. Langhoff, T. C. Steimle, and J. E. Shirley, J. Chem. Phys. **93**, 4179 (1990).
[68] K. C. Namiki, J. S. Robinson, and T. C. Steimle, J. Chem. Phys. **109**, 5283 (1998).
[69] R. Sievert, I. Cadez, J. Van-Doren, and A. W. Castleman Jr, J. Phys. Chem. **88**, 4502 (1984).
[70] T. C. Steimle, J. H. Chen, and J. Gengler, J. Chem. Phys. **121**, 829 (2004).
[71] V. J. Barclay, J. C. Polanyi, Y. Zeiri, and R. Kosloff, J. Chem. Phys. **98**, 9185 (1993).
[72] L. G. M. Pettersson, P. E. M. Siegbahn, and S. Ismail, Chem. Phys. **82**, 355 (1983).
[73] J. K. Agreiter, A. M. Knight, and M. A. Duncan, Chem. Phys. Lett. **313**, 162 (1999).
[74] H. Martin, J. Chem. Phys. **88**, 1797 (1988).
[75] A. Carrington, C. A. Leach, A. J. Marr, A. M. Shaw, M. R. Viant, J. M. Hutson, and M. M. Law, J. Chem. Phys. **102**, 2379 (1995).
[76] K. P. Huber and G. Herzberg, *Molecular Spectra and Molecular Structure. IV. Constants of Diatomic Molecules* (Van Nostrand Reinhold, New York, 1979).
[77] C. Jamorski, A. Dargelos, C. Teichteil, and J. P. Daudey, J. Chem. Phys. **100**, 917 (1994).
[78] K. Balasubranian, J. Chem. Phys. **93**, 8061 (1990).
[79] A. B. Alekseyev, H. P. Liebermann, R. J. Buenker, and G. Hirsch, J. Chem. Phys. **104**, 4672 (1996).
[80] H. Birk, R. D. Urban, P. Polomsky, and H. Jones, J. Chem. Phys. **94**, 5435 (1991).
[81] R. C. Weast, M. J. Astle, and W. H. Beyer, *Handbook of Chemistry and Physics*, 65th ed., 1984–1985 (CRC, Boca Raton, Florida, 1984).
[82] D. P. Baldwin, M. A. Buntine, and D. W. Chandler, J. Chem. Phys. **93**, 6578 (1990).
[83] D. R. Herrick and F. H. Stillinger, J. Chem. Phys. **62**, 4360 (1975).
[84] J. E. Huheey, E. A. Keiter, and R. L. Keiter, *Inorganic Chemistry*, 4th ed. (Harper Collins, New York, 1993), p. 41.

[85] Y. Nosenko, M. Kunitski, R. P. Thummel, A. Kyrychenko, J. Herbich, J. Waluk, C. Riehn, and B. Brutschy, J. Am. Chem. Soc. **128**, 10000 (2006).
[86] H. Busener, F. Heinrich, and A. Hese, Chem. Phys. **112**, 139 (1987).
[87] R. N. Diffenderfer and D. R. Yarkony, J. Phys. Chem. **86**, 5098 (1982).
[88] J. F. Harrison, R. W. Field and C. C. Jarrold, in *ACS Symposium Series* edited by M. R. Hofmann and G. DyallK (Volume 828, ACS, Washington, 2002), Chapter 11, p. 28.
[89] D. Bellert, D. K. Winn, and W. H. Breckenridge, J. Chem. Phys. **117**, 3139 (2002).
[90] J. Koput and K. A. Peterson, J. Chem. Phys. **116**, 9255 (2002).
[91] A. Buchler, L. Wharton, J. L. Stauffer, and W. Klemperer, J. Chem. Phys. **39**, 2299 (1963).
[92] D. Bellert, D. K. Winn, and W. H. Breckenridge, J. Chem. Phys. **119**, 10169 (2003).
[93] A. I. Boldyrev and P. V. Schleyer, J. Am. Chem. Soc. **113**, 9045 (1991).
[94] A. Boldyrev, private communication.
[95] G. A. Bishea and M. D. Morse, J. Chem. Phys. **95**, 5646 (1991).
[96] K. K. Das and K. Balasubramanian, J. Mol. Spectrosc. **140**, 280 (1990).
[97] W. C. Ermler, Y. S. Lee, and K. S. Pitzer, J. Chem. Phys. **70**, 293 (1979).
[98] K. R. Wilson and D. R. Herschbach, J. Chem. Phys. **49**, 2676 (1968).
[99] R. D. Levine, *Molecular Reaction Dynamics* (Cambridge University Press, UK, 2004).
[100] M. F. Vernon, H. Schmidt, P. S. Weiss, M. H. Covinsky, and Y. T. Lee, J. Chem. Phys. **84**, 5580 (1986).
[101] J. M. Mestdagh, B. A. Balko, M. H. Covinsky, P. S. Weiss, M. F. Vernon, H. Schmidt, and Y. T. Lee, Faraday Discuss. **84**, 145 (1987).
[102] M. G. Prisant, C. T. Rettner, and R. N. Zare, J. Chem. Phys. **81**, 2699 (1984).
[103] M. Cizek, J. Horacek, and W. Domcke, Phys. Rev. A **60**, 2873 (1999).
[104] R. Düren, U. Lackschewitz, S. Miloevi, and H. J. Waldapfel, J. Chem. Soc., Faraday Trans. **2 85**, 1017 (1989).
[105] R. Düren, U. Lackschewitz, and S. Milosevic, Chem. Phys. **126**, 81 (1988).
[106] X. Y. Chang, R. Ehlich, A. J. Hudson, P. Piecuch, and J. C. Polanyi, Faraday Discuss **108**, 411 (1997).
[107] C. T. Rettner and R. N. Zare, J. Chem. Phys. **77**, 2416 (1982).
[108] B. Soep, S. Abbes, A. Keller, and J. P. Visticot, J. Chem. Phys. **96**, 440 (1992).
[109] M. L. Dubernet and J. M. Hutson, J. Chem. Phys. **101**, 1939 (1994).
[110] B. Soep, S. Abbes, A. Keller, and J. P. Visticot, J. Chem. Phys. **96**, 440 (1992).
[111] P. R. Brooks and E. M. Jones, J. Chem. Phys. **45**, 3449 (1966).
[112] D. H. Parker, K. K. Chakravorty, and R. B. Bernstein, J. Phys. Chem. **85**, 466 (1981).
[113] S. E. Choi and R. B. Bernstein, J. Chem. Phys. **83**, 4463 (1985).
[114] H. J. Loesch and J. Moller, J. Phys. Chem. A. **101**, 7534 (1997).
[115] M. H. M. Janssen, D. H. Parker, and S. Stolte, J. Phys. Chem. **95**, 8142 (1991).
[116] A. Keller, R. Lawruszczuk, B. Soep, and J. P. Visticot, J. Chem. Phys. **105**, 4556 (1996).
[117] E. R. Fisher and G. K. Smith, Appl. Opt. **10**, 1803 (1971).
[118] E. Bauer, E. R. Fisher, and F. R. Gilmore, J. Chem. Phys. **51**, 4173 (1969).
[119] W. H. Breckenridge and H. Umemoto, *The Dynamics of the Excited State* (Wiley, New York, 1982), Vol. 50.
[120] G.-H. Jeung, H. S. Lee, K. H. Kim, and Y. S. Lee, Chem. Phys. Lett. **358**, 151 (2002).
[121] W. Reiland, H. U. Tittes, I. V. Hertel, V. Bonacic-Koutecky, and M. Persico, J. Chem. Phys. **77**, 1908 (1982).
[122] W. H. Breckenridge, C. Jouvet, and B. Soep, J. Chem. Phys. **84**, 1443 (1986).
[123] C. Jouvet and B. Soep, Chem. Phys. Lett. **96**, 426 (1983).
[124] J. C. Polanyi and J.-X. Wang, J. Phys. Chem. **99**, 13691 (1995).
[125] C. Blondel, C. Delsart, and F. Goldfarb, J. Phys. B. - Atomic Molecular and Optical Physics **34**, L281–L288 (2001).
[126] A. J. Hudson, H. B. Oh, J. C. Polanyi, and P. Piecuch, J. Chem. Phys. **113**, 9897 (2000).

[127] S. Skowronek, R. Pereira, and A. GonzalezUrena, J. Phys. Chem. A **101**, 7468 (1997).
[128] P. Farmanara, V. Stert, W. Radloff, S. Skowronek, and A. Gonzalez-Urena, Chem. Phys. Lett. **304**, 127 (1999).
[129] J. M. Mestdagh, F. Spiegelman, E. Gloaguen, M. Collier, F. Lepetit, M. A. Gaveau, C. S. Sanz, and B. Soep, J. Phys. Chem. A **110**, 7355 (2006).
[130] M. A. Gaveau, E. Gloaguen, P. R. Fournier, and J. M. Mestdagh, J. Phys. Chem. A **109**, 9494 (2005).
[131] E. Gloaguen, C. S. Sanz, M. Collier, M. A. Gaveau, B. Soep, O. Roncero, and J. M. Mestdagh, J. Phys. Chem. A **112**, 1408 (2008).
[132] J. M. Mestdagh, F. Spiegelman, E. Gloaguen, M. Collier, F. Lepetit, M. A. Gaveau, C. S. Sanz, and B. Soep, J. Phys. Chem. A **110**, 7355 (2006).
[133] L. M. Blomberg, M. R. A. Blomberg, and P. E. M. Siegbahn, J. Inorg. Biochem. **99**, 949 (2005).
[134] S. Patchkovskii, P. M. Kozlowski, and M. Z. Zgierski, J. Chem. Phys. **121**, 1317 (2004).
[135] J. W. Petrich and J. L. Martin, Chem. Phys. **131**, 31 (1989).
[136] R. Kumble, G. R. Loppnow, S. Hu, A. Mukherjee, M. A. Thompson, and T. G. Spiro, J. Phys. Chem. B **99**, 5809 (1995).
[137] M. Gouterman, in *The Porphyrins*, edited by D. H. Dolphin (Academic Press, New York, 1978), Vol. III, p. 1.
[138] S. Sorgues, L. Poisson, K. Raffael, L. Krim, B. Soep, and N. Shafizadeh, J. Chem. Phys. **124**, 114302 (2006).
[139] H. Z. Yu, J. S. Baskin, B. Steiger, C. Z. Wan, F. C. Anson, and A. H. Zewail, Chem. Phys. Lett. **293**, 1 (1998).
[140] M. S. Liao and S. Scheiner, J. Chem. Phys. **117**, 205 (2002).
[141] J. Rodriguez and D. Holten, J. Chem. Phys. **91**, 3525 (1989).
[142] Y. Mitzutani, Y. Uesugi, and T. Kitagawa, J. Chem. Phys. **111** (19), 8950 (1999).
[143] S. Villaume, A. Strich, C. Daniel, S. A. Perera, and R. J. Bartlett, Phys. Chem. Chem. Phys. **9**, 6115 (2007).
[144] K. Pierloot, E. Tsokos, and L. G. Vanquickenborne, J. Phys. Chem. **100**, 16545 (1996).
[145] J. Itatani, J. Levesque, D. Zeidler, H. Niikura, H. Pepin, J. C. Kieffer, P. B. Corkum, and D. M. Villeneuve, Nature **432**, 867 (2004).
[146] W. Boutu, S. Haessler, H. Merdji, P. Breger, G. Waters, M. Stankiewicz, L. J. Frasinski, R. Taieb, J. Caillat, A. Maquet, P. Monchicourt, B. Carre, and P. Salieres, Nature Phys. **4**, 545 (2008).
[147] F. Remacle and R. D. Levine, Proc. Natl. Acad. Sci. USA **103**, 6793 (2006).